Neutrophil membrane fusogenic nanoliposomal leonurine for targeted ischemic stroke therapy via remodeling cerebral niche and restoring blood-brain barrier integrity

Zhuang Tang [a], Shiyu Meng [a], Zhiling Song [a], Xiaoxue Yang [a], Xinzhi Li [a], Hui Guo [b], Meirong Du [a,c], Jun Chen [d], Yi Zhun Zhu [a,*], Xiaolin Wang [a,**]

[a] School of Pharmacy and State Key Laboratory of Quality Research in Chinese Medicine, Macau University of Science and Technology, Macao 999078, China
[b] School of Chemical Engineering and Technology, Sun Yat-sen University, Zhuhai 519082, China
[c] NHC Key Lab of Reproduction Regulation (Shanghai Institute of Planned Parenthood Research), Shanghai Key Laboratory of Female Reproductive Endocrine Related Diseases, Hospital of Obstetrics and Gynecology, Fudan University Shanghai Medical College, Shanghai 200032, China
[d] School of Pharmacy, Fudan University, Shanghai 201203, China

ARTICLE INFO

ABSTRACT

Ischemic stroke (IS) constitutes the leading cause of global morbidity and mortality. Neuroprotectants are essential to ameliorate the clinical prognosis, but their therapeutic outcomes are tremendously compromised by insufficient delivery to the ischemic lesion and intricate pathogenesis associated with neuronal damage, oxidative stress, inflammation responses, blood-brain barrier (BBB) dysfunction, *etc*. Herein, a biomimetic nanosystem (Leo@NM-Lipo) composed of neutrophil membrane-fused nanoliposomal leonurine (Leo) is constructed, which can not only efficiently penetrate and repair the disrupted BBB but also robustly remodel the harsh cerebral microenvironment to reverse ischemia-reperfusion (I/R) injury. More specifically, the neutrophil membrane inherits the BBB penetrating, infarct core targeting, inflammation neutralization, and immune evasion properties of neutrophils, while Leo, a naturally occurring neuroprotectant, exerts pleiotropic effects to attenuate brain damage. Remarkably, comprehensive investigations disclose the critical factors influencing the targetability and therapeutic performances of biomimetic nanosystems. Leo@NM-Lipo with a low membrane protein-to-lipid ratio of 1:10 efficiently targets the ischemic lesion and rescues the injured brain by alleviating neuronal apoptosis, oxidative stress, neuroinflammation, and restoring BBB integrity in transient middle cerebral artery occlusion (tMCAO) rats. Taken together, our study provides a neutrophil-mimetic nanoplatform for targeted IS therapy and sheds light on the rational design of biomimetic nanosystems favoring wide medical applications.

1. Introduction

Ischemic stroke (IS) is a fatal cerebrovascular event caused by the sudden interruption of cerebral blood circulation, which constitutes the leading cause of mortality and acquired disability worldwide [1]. Immediately after ischemia, neurons are deprived of oxygen and energy, failing to sustain normal transmembrane ionic gradient and homeostasis. Consequently, cascades of pathological events including excitotoxicity, oxidative and nitrative stress, inflammation, and apoptosis are initiated, which are closely linked and mutually intensified [2]. Clinical interventions such as intravenous thrombolysis with recombinant tissue plasminogen activator (tPA) and surgical thrombectomy can re-establish

the blood supply, which is essential to salvage ischemic penumbra [3]. However, the rapid increase of tissue oxygenation and glucose induces a second burst of reactive oxygen species (ROS) generation to elicit ischemia-reperfusion (I/R) injury, which leads to blood-brain barrier (BBB) damage, vasogenic edema, and secondary inflammation insult to the brain parenchyma [4–6]. Therefore, it is imperative to explore new treatments for efficient neuroprotection.

Despite extensive investigations in the past decades, there is still a lack of neuroprotective agents in the clinical realm [7]. With a long history of more than 2000 years in clinical use, Chinese herbal medicine-derived active gradients represent an alternative for IS management owing to the multitargeted and multileveled intervention effects

[8,9]. Among them, Leonurine (Leo), a unique alkaloid derived from *Herba Leonuri,* has been investigated in depth due to its pleiotropic properties including antioxidation, anti-inflammation, and anti-apoptosis [10]. Our previous investigations demonstrated that Leo can efficiently scavenge ROS to prevent IS progression by restoring mitochondrial function and the redox state of the ischemic brain [11]. Excitingly, Leo exerted superior anti-I/R effects than the classical neuroprotectant Edaravone in stroke rats, and the cerebral infarct volume and neurological deficit score in the Leo group was 65.2% and 80.7% that of the Edaravone group after 72 h treatment [12]. Besides, Leo can also protect the brain against oxidative stress and neuronal damage [13] and downregulate neuroinflammation to attenuate neurological impairments [14]. However, the therapeutic potentials of neuroprotectants including Leo are compromised by the poor BBB penetrating and lesion targeting capability, along with inadequate interactions with the intricate pathological microenvironment. Therefore, the development of a multi-faceted drug delivery system is in urgent need [15].

Cell membrane coating nanotechnology is an emerging "top-down" functionalization strategy by nesting cell membranes from specific cells (*e.g.* leukocytes, platelets, erythrocytes) to the surface of synthetic substrates (*e.g.* liposomes, polymeric nanoparticles, metal nanoparticles) [16,17]. The resulting nanosystems are bestowed with cell-like properties and can interact with complex biological or pathological microenvironments, which can considerably facilitate penetration through various biological barriers including the BBB while avoiding undesired immune responses [18]. In the pathogenesis of IS, neutrophils are the first and most abundant leukocyte subpopulation to infiltrate the ischemic brain by interacting with up-regulated intercellular adhesion molecule-1 (ICAM-1) and vascular cell adhesion molecule-1 (VCAM-1) on inflammatory brain microvascular endothelial cells via membrane proteins including integrin β2, platelet endothelial cell adhesion molecules-1 (PECAM-1) and CD11b [19]. Afterward, neutrophils migrate through the endothelial vessel wall and are attracted toward the ischemic area by chemokines, releasing proinflammatory factors, ROS, proteases, and matrix metalloproteinases (MMPs) to exacerbate brain injury [20]. Therefore, neutrophils constitute ideal cell membrane donors for the management of inflammatory brain disorders [21–23]. On the one hand, neutrophil membrane-coated nanoagents can penetrate BBB and translocate to inflammatory lesions through affinity between neutrophil surface antigen and upregulated adhesion markers (*e.g.* ICAM-1, VCAM-1) and chemokines (*e.g.* CXCL2, CXCL12) [21,23]. On the other hand, instead of releasing detrimental factors to exacerbate brain damage, these neutrophil decoys can neutralize inflammation by adsorbing inflammatory cytokines (*e.g.* TNF-α, IL-1β, IL-6) and inhibit neutrophil infiltration to remodel the inflammatory microenvironment [24].

Herein, we propose a neutrophil-mimetic nanoplatform for non-invasive intracerebral drug delivery by translocating the neutrophil-like human promyelocytic leukemia (HL-60) cell-derived membranes (NM) onto the surface of Leo-loaded nanoliposomes (Lipo) with different weight ratios. The resulting proteolipid vesicles (Leo@NM-Lipo) retain the potent drug delivery properties of liposomal formulations while conferred with selective and effective drug delivery to the infarcted brain mediated by abundant membrane proteins (Scheme 1). It is worth mentioning that neutrophil membrane cloaking not only navigates the cargo transport to the lesion but also achieves synergistic anti-inflammation effects with Leo due to its high affinity to inflammatory cytokines. So far, the key factors influencing the biointerfacing performance of cell membrane-camouflaged nanosystems remain rarely explored [18,25]. In this paper, we demonstrate that the cell membrane-to-nanocore weight ratio not only modifies the physicochemical properties but also tremendously impacts the targetability and therapeutic outcomes of biomimetic nanoagents, evidenced by systematic investigations both *in vitro* and *in vivo*. Leo@NM-Lipo fabricated with a low cell membrane protein-to-lipid ratio of 1:10 significantly improves
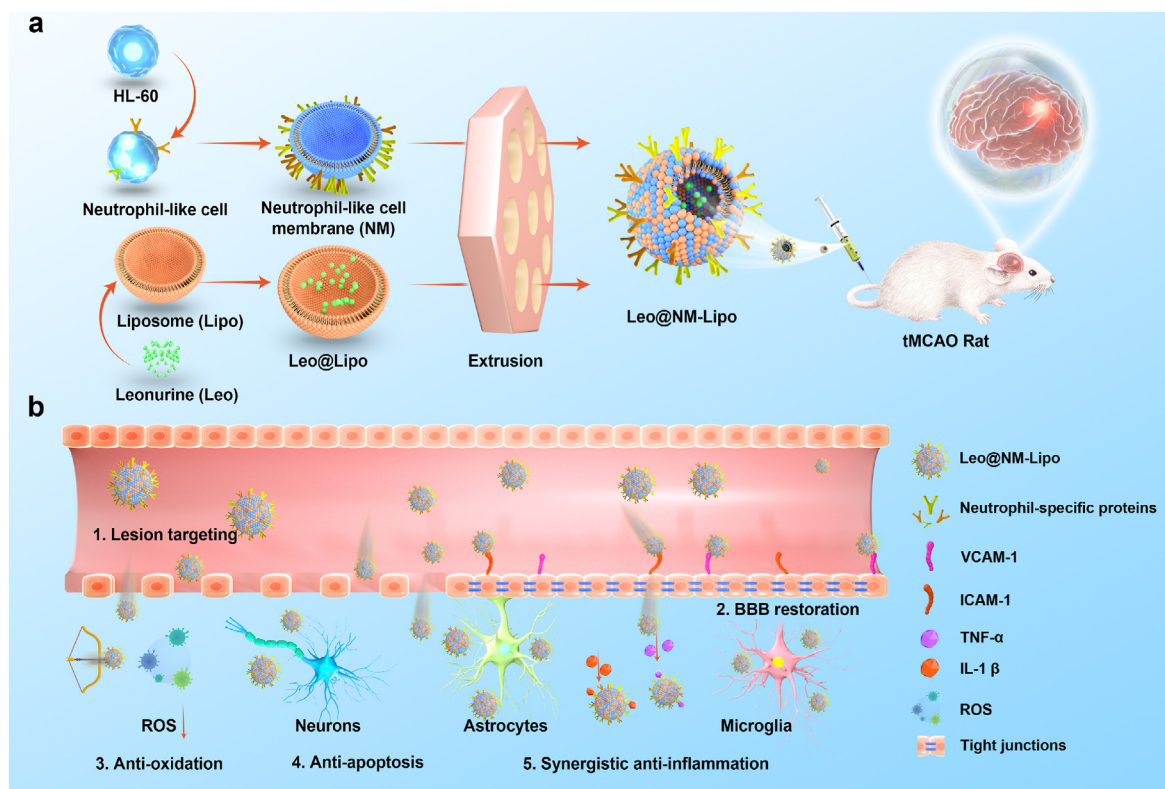
Scheme 1. Illustration of a neutrophil-inspired nanoplatform Leo@NM-Lipo for targeted ischemic stroke therapy. **(a)** Fabrication procedure of Leo@NM-Lipo. **(b)** Intravenous injection of Leo@NM-Lipo achieved efficient reversal of cerebral ischemia-reperfusion injury through lesion targeting, ROS scavenging, neuronal apoptosis inhibition, inflammation resolution, and BBB integrity restoration.

the delivery efficiency of Leo across BBB to exert anti-oxidant, anti-inflammatory, and anti-apoptotic effects to alleviate brain damage in tMCAO rats with significantly reduced infarct volume and ameliorated neurological recovery. This strategy integrates accurate lesion homing, boosted therapeutic efficacy, along with excellent industrial prospects thus holds great promise to promote clinical translation of therapeutic payloads favoring the treatment of a wide range of inflammation-dominated diseases including brain disorders.

2. Results

2.1. Construction and characterization of Leo@NM-Lipo

Leo@NM-Lipo was constructed through the membrane fusion technique (Scheme 1a). More specifically, liposomes (Lipo) were first prepared through a thin film hydration-extrusion approach whilst Leo was encapsulated in the aqueous core through a pH-gradient method. To obtain neutrophil membrane (NM), HL-60 cells were first induced to differentiation by a combination of dimethylsulfoxide (DMSO) and TNF-α to obtain inflammation-activated neutrophil-like cells, the nucleus of which became polymorphic, horseshoe and kidney-shaped (Fig. S1). Meanwhile, membrane protein expressions including CD11b, PECAM-1, and Integrin-β2 were remarkably up-regulated compared with the undifferentiated counterpart (Fig. S2), all of which were involved in the cell adhesion and migration of the neutrophils to the infarcted brain.

Successful translocation of NM was characterized by the morphology, size, zeta potential, and key membrane proteins. As manifested in Fig. 1a, the morphology of the nanovesicles was observed by transmission electron microscopy (TEM), in which Lipo was in the shape of regular spheres while NM-Lipo and Leo@NM-Lipo exhibited a typical core-shell structure of liposome core and neutrophil membrane layer, indicating the successful camouflaging of the neutrophil membrane [26]. Dynamic light scattering (DLS) measurements disclosed that bare liposomes were sized at 93 nm while the diameter of NM-Lipo and Leo@NM-Lipo was elevated to ~103 nm (Fig. 1b). Meanwhile, the zeta potential of Leo@NM-Lipo was −24.2 ± 0.1 mV, varied between pure NM and bare liposomes, which were −29.2 ± 0.7 mV and −20.2 ± 0.6 mV respectively (Fig. 1c).

The protein profiles in NM and NM-Lipo were determined by sodium dodecyl sulfate-polyacrylamide gel electrophoresis (SDS-PAGE) assay. As demonstrated in Fig. 1d, the protein composition in neutrophil-like cell membrane was mostly retained in NM-Lipo whereas no protein signal was detected in bare Lipo. Furthermore, western blots (WB) were conducted to confirm the preservation of key membrane proteins including lymphocyte function-associated antigen 1 (LFA-1, also known as CD 11a/CD18), CD 11b, IL-1β receptor (IL-1R) and TNF-α receptor (TNF-αR), PECAM, integrin β2 after derivation and camouflaging (Fig. 1e). Fluorescent NM-Lipo was constructed with NM labeled by DiO and Lipo labeled by DiD. After incubation with activated BCECs, the two constituents were distinguished with a confocal microscope. Co-location analysis by ImageJ revealed that the overlap coefficient was 0.93, confirming
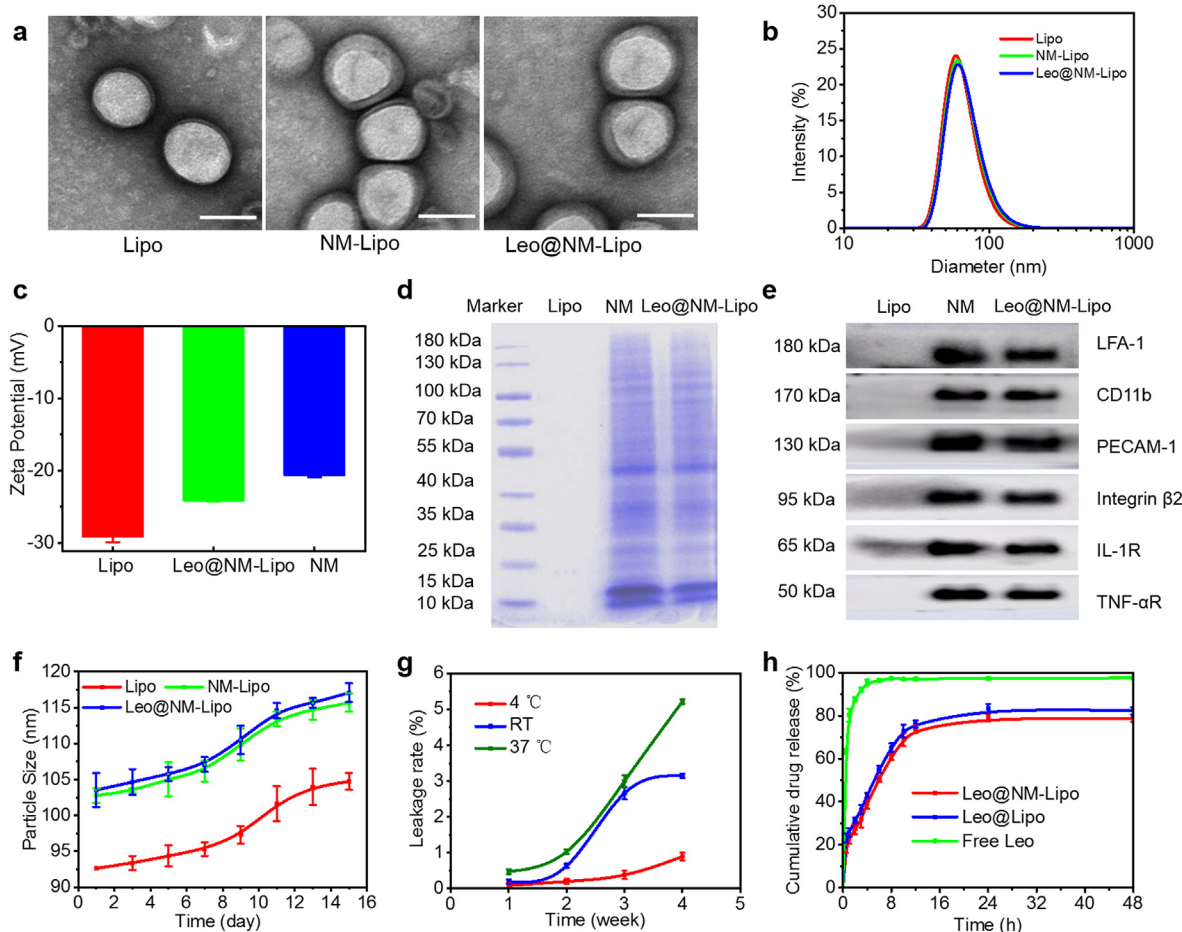
Fig. 1. Characterizations of Leo@NM-Lipo. **(a)** Morphology of Lipo, NM-Lipo, and Leo@NM-Lipo observed by transmission electron microscopy, scale bar = 100 nm). **(b)** Hydrodynamic sizes and **(c)** Zeta potential of Lipo, NM-Lipo, and Leo@NM-Lipo. **(d)** SDS-PAGE and **(e)** western blotting analysis of the characteristic proteins from Lipo, NM-Lipo, and Leo@NM-Lipo. **(f)** The stability of Lipo, NM-Lipo, and Leo@NM-Lipo in PBS (10 mM, pH = 7.4) at 4 °C monitored by DLS over 15 days. **(g)** Leakage of Leo@NM-Lipo at 4 °C, 37 °C, and room temperature (RT) for 4 weeks. **(h)** The drug release profile of free Leo, Leo@Lipo, and Leo@NM-Lipo in 10 mM PBS at 37 °C. Data were expressed as mean ± SD, n = 3.

the perfect integration of NM and Lipo (Fig. S3). Therefore, important functional proteins engaged in inflammation tropism and inflammatory factors sequestering were well translocated to the surface of Leo@NM-Lipo.

Leonurine (Leo) has poor solubility both in water and organic solvent and the solubility in water is pH dependent [27]. Therefore, Leo was loaded into the aqueous core of Lipo by the pH gradient method, with the pH of inside and outside liposomes adjusted to be 4.0 and 7.0 respectively. Along the pH gradient, Leo can cross the phospholipid membrane in the form of molecules and readily be enclosed in the internal aqueous phase in the form of ions. To optimize the formulation, Leo was added to Lipo suspension at different weight ratios (Fig. S4). The loading efficiency (LE%) and encapsulation efficiency (EE%) of the optimal formulation at 1:5 (Leo: Lipo) were determined to be 13.6% $\pm$ 0.36% and 78.51% $\pm$ 0.21%, respectively. Interestingly, the as-obtained formulation exhibited excellent storage stability. Specifically, the particle diameters of Lipo and NM-Lipo barely changed within 15 days in PBS at 4 °C (Fig. 1f). The particle size of Lipo, NM-Lipo and Leo@NM-Lipo barely changed in pH 5.0, 6.0 and 7.4, indicating that the platform was stable in different pH (Table S1). Moreover, the leakage rates of Leo@NM-Lipo were <5 wt% even stored at a temperature as high as 37 °C for one month, probably due to the high phase transition temperature of DPPC, which can maintain structural integrity below 41 °C (Fig. 1g) [28]. Drug release profiles of free Leo, Leo@Lipo, and Leo@NM-Lipo were monitored in PBS at 37 °C (Fig. 1h). Free Leo was readily released within 4 h. In contrast, Leo@NM-Lipo exhibited a first-order kinetic release profile up to 24 h (Table S2), which was distinct from Leo ($f_2 = 18.63$) and slightly retarded than Leo@Lipo ($f_2 = 70.03$), assuring potentially prolonged therapeutic effect *in vivo*.

2.2. Therapeutic potential in vitro

Neutrophil-mimetic nanoagents were expected to mimic natural neutrophils to sequester proinflammatory cytokines [24]. Thereafter, the binding ability of Leo@NM-Lipo with TNF-α and IL-1β was explored. As presented in Fig. 2a and b, the level of TNF-α and IL-1β showed no variations with the concentration of bare Lipo increasing from 32 to 4096 μg mL^{-1}. In sharp contrast, Leo@NM-Lipo containing different membrane protein-to-lipid weight ratios (1:1, 1:10, 1:100, 1:500) witnessed robust TNF-α and IL-1β absorbing ability in a concentration-dependent manner. Notably, the IC$_{50}$ (half maximal inhibitory concentration) determined using the Hill equation in the 1:10 group was as low as 122.1 μg mL^{-1} for TNF-α binding (Fig. 2a) and 85.6 μg mL^{-1} for IL-1β binding (Fig. 2b) based on the measured binding kinetic profiles, suggesting potent inflammation neutralization ability.

Furthermore, an oxygen-glucose deprivation/reoxygenation (OGD/R) model was established to evaluate the protective effect of Leo@NM-Lipo against oxidative stress, neuronal damage, and BBB dysfunction (Fig. 2c). More specifically, the OGD/R-induced ROS production in PC12 cells seeded in the lower chamber was detected by the fluorescent probe DCFHDA (Fig. 2d). After OGD/R treatment, PC12 cells were observed with significantly elevated fluorescence intensity, which was decreased by 26.1%, 29.1%, and 37.5% after treatments with Leo, Leo@Lipo, and Leo@NM-Lipo respectively (Fig. 2e). Besides, the survival rate of PC12 cells after OGD/R treatment declined dramatically to 43.1% while Leo, Leo@Lipo, and Leo@NM-Lipo enhanced the viability to 67.0%, 70.1%, and 75.6% that of the control group, respectively (Fig. 2f). Furthermore, the transepithelial electrical resistance (TEER) of BCECs in the upper chamber was monitored to evaluate the integrity of BCECs monolayer in a non-destructive manner (Fig. 2g) [29]. The TEER of the control group increased steadily to ~110%. In comparison, the TEER of OGD/R treated groups decreased to ~90% after OGD/R treatment and recovered slowly 24 h after reoxygenation, among which the Leo@NM-Lipo group witnessed the most rapid and highest recovery rate to 103.2% of the initial level.

To evaluate the safety of Leo@NM-Lipo, a hemolysis assay was performed by co-incubating nanoliposomes with 2% red blood cell (RBC) suspension for 3 h, which demonstrated that Leo@NM-Lipo exerted minimal hemolytic rate (<5%) in the range of 10–1000 μg mL^{-1} (Fig. 2h). In addition, the viability of BCECs and PC12 cells after 24 h co-incubation with Leo@NM-Lipo was evaluated by CCK-8 test. Resultantly, Leo@NM-Lipo exhibited negligible cytotoxicity even at a concentration as high as 2000 μg mL^{-1} (cell viability >80%) (Fig. 2i and j). Overall, the *in vitro* evaluations implicated that Leo@NM-Lipo significantly enhanced the therapeutic effects of free Leo along with desirable biocompatibility, and therefore holds great potential for the treatment of cerebral ischemia.

## 2.3. Targeting inflamed cerebral vasculature and penetration across BBB in vitro

To study the selective targeting effect of NM-Lipo on the inflammatory BBB, BCECs were activated by TNF-α to upregulate the expression of adhesion proteins ICAM-1 and VCAM-1 (Fig. S6). After co-incubation with DiD-labeled NM-Lipos with different membrane protein-to-lipid weight ratios, the red fluorescent signals ascended positively correlated with NM ratios (Fig. 3a–d and Fig. S7), which was ascribed to the enhanced interaction between CD11b, PECAM-1 and integrin β2 on NM and ICAM-1 and VCAM-1 on BCECs [30]. The stereotaxis image analysis revealed that the existence of NM substantially enhanced the cellular uptake efficiency (Fig. 3b and c). Besides, we compared the binding ability of NM-Lipo to BCECs with or without TNF-α treatment to study the selective targetability to inflammatory BBB. The results showed that the fluorescence signals of DiD-labeled bare Lipo were similar in BCECs with or without activation, indicating indiscriminate cellular uptake. On the contrary, the internalization of NM-Lipo in inflammatory BCECs was enhanced to 3.02-fold that of bare Lipo and 1.67-fold that of NM-Lipo in non-activated cells (Fig. S8a and b).

The BBB penetrating ability was evaluated in a transwell-mediated BBB model with BCECs in the upper insert and PC12 cells in the lower chamber as receptor cells (Fig. 3e). The cellular uptake of NM-Lipos composed of various membrane protein-to-lipid ratios by BCECs and PC12 cells was also quantified with flow cytometry and the results were consistent with confocal observations (Fig. 3f and g). Meanwhile, we also compared the transcytosis of NM-Lipo through BCECs with or without TNF-α treatment. Interestingly, the fluorescent intensity of NM-Lipo penetrating across inflammatory BCECs was 2.28-fold that of bare Lipo and 1.37-fold that of NM-Lipo through non-activated BCECs layers (Fig. S9a and b). These data confirmed that NM-Lipo can selectively target inflammatory BBB and be subsequently internalized by neural cells.

2.4. Prolonged plasma circulation and preferential targeting to ischemic brain

Healthy SD rats were intravenously administered with Lipo-DiD and NM-Lipo-DiD to evaluate the *in vivo* elimination kinetics. The blood samples were collected at predetermined time points for imaging and the fluorescence intensity measurement (Fig. 4a and b). The results showed that the Lipo core alone also exhibited prolonged plasma retention due to the presence of PEG on the surface [31]. NM-Lipo-DiD was observed with a slightly lower clearance rate than Lipo-DiD, probably due to the immune-evasion effect of the NM coating [32].

To verify the lesion-targeting capability of the nanoplatforms, tMCAO model rats were intravenously injected with DiD-labeled Lipo, and NM-Lipos made from different membrane protein-to-lipid weight ratios (0:1, 1:1, 1:10, 1:100) 0.5 h post-reperfusion. The main organs including the brain, heart, liver, spleen, lung, and kidney were collected and underwent ex vivo fluorescent imaging at 6 h post injection (Fig. 4c). As demonstrated in Fig. 4d and e, NM-decorated nanoagents substantially enhanced enrichment at the ischemic lesion, among which NM-Lipo-DiD (1:10) group and NM-Lipo-DiD (1:1) exhibited comparable intracerebral
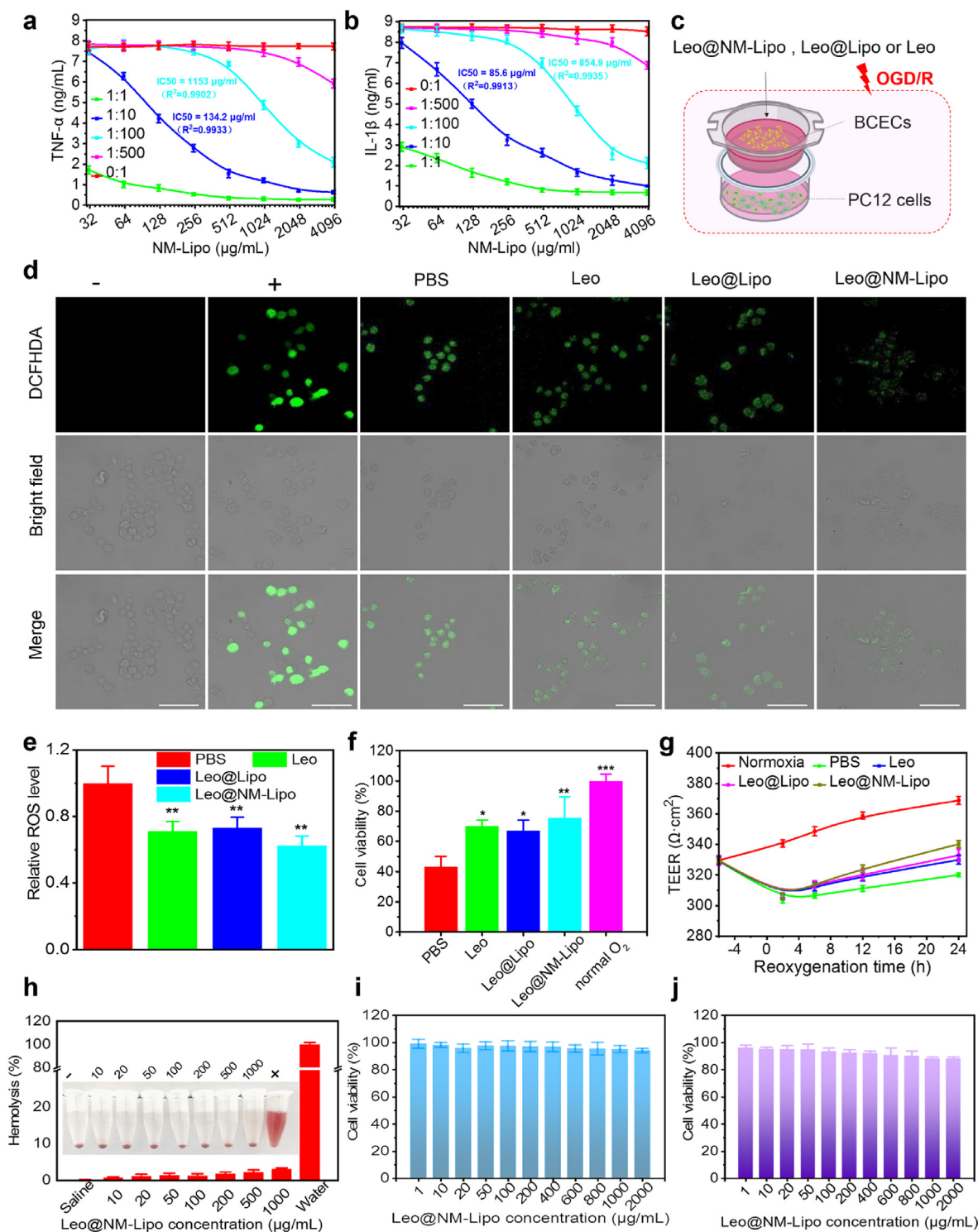
Fig. 2. *In vitro* therapeutic efficacy and hemo/cytocompatibility. Inflammation neutralization capability of Leo@NM-Lipo with various membrane protein-to-lipid ratios via absorbing inflammatory cytokines **(a)** TNF-α and **(b)** IL-1β. Nonlinear regression fitting with an inhibitory dose-response model (variable slope model) was employed and processed by Graphpad Prism 9. **(c)** Setup of OGD/R treatment. **(d)** ROS elimination in PC12 cells in OGD/R model after different treatments (Scale bar = 50 μm). **(e)** Corresponding quantification of fluorescence intensity. **(f)** Cell viability of PC12 cells after OGD/R treatment. **(g)** TEER of BBB monolayer *in vitro* before and after OGD/R treatment. **(h)** Hemolysis percentage and images of RBCs incubated with Leo@NM-Lipo for 3 h. Saline and distilled water were used as negative and positive controls, respectively. Cell viability of **(i)** BCECs and **(j)** PC12 cells was determined with CCK-8 tests after incubation with different concentrations of Leo@NM-Lipo. Data represent mean ± SD, n = 3. Variance among groups was determined by one-way ANOVA with Tukey multiple comparisons posthoc test (*$p < 0.05$, **$p < 0.01$, ***$p < 0.001$).
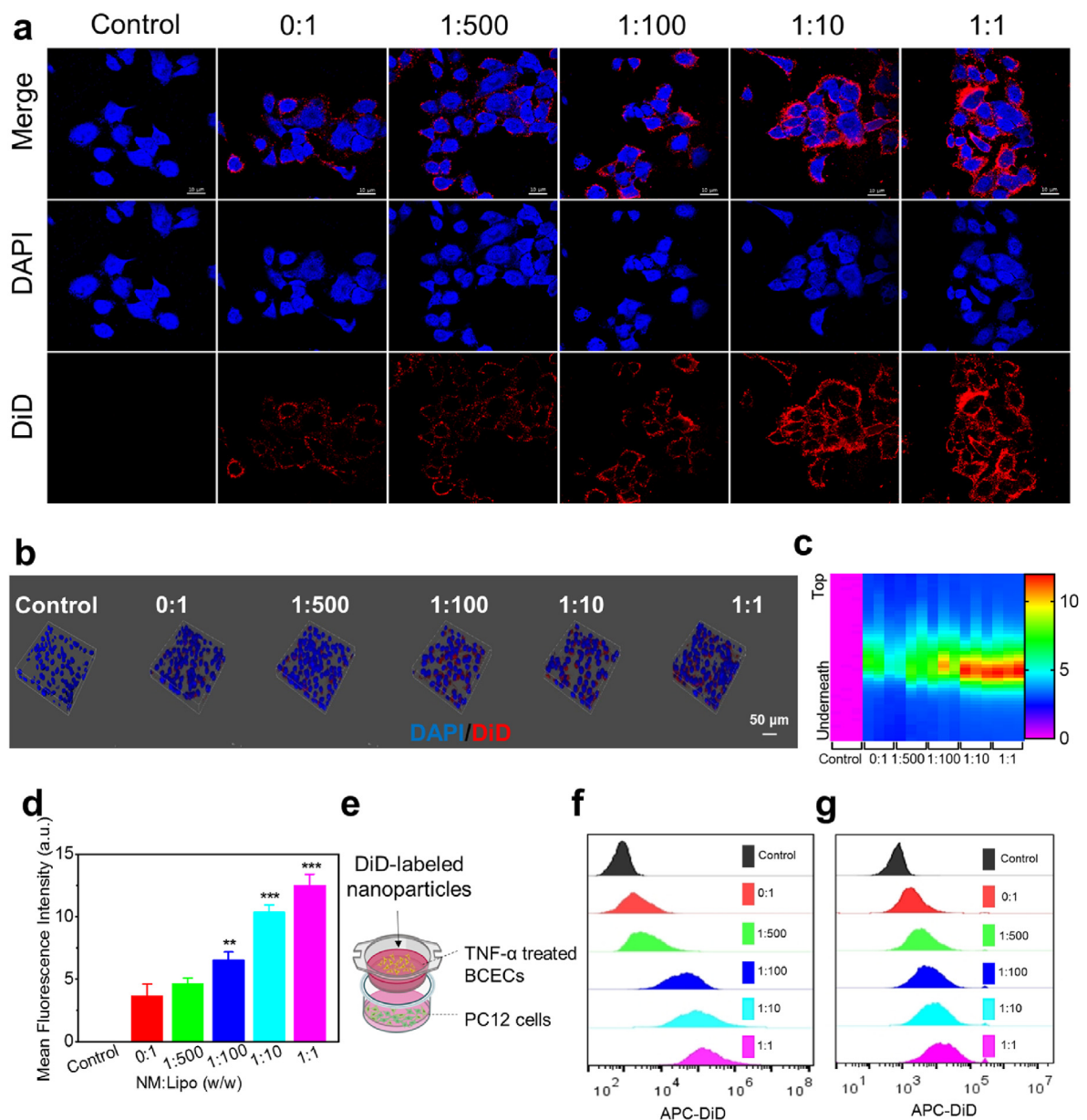
Fig. 3. *In vitro* targeting and penetration across BBB. **(a)** cellular uptake of NM-Lipo at cell membrane protein-to-lipid ratio 0:1, 1:500, 1:100, 1:10, and 1:1 by inflammatory BCECs. **(b)** 3D scanning of BCECs incubated with NM-Lipo with various NM-to-Lipo ratios. **(c)** The distribution analysis of NM-Lipo with various membrane protein-to-lipid ratios in BCECs. **(d)** Quantitative of the stereotaxis. **(e)** Setup of DiD-labeled nanocarrier transcytosis for PC12 cell internalization. Endocytosis of NM-Lipo with various NM to Lipo ratios by **(f)** BCECs and **(g)** PC12 cells. Data represent mean ± SD, n = 3. Variance among groups was determined by one-way ANOVA with Tukey multiple comparisons post-hoc test (**$p < 0.01$, ***$p < 0.001$).

delivery efficiency. Besides, the fluorescent intensity in ipsilateral brain tissues of all the groups peaked 6 h post-injection, and NM-Lipos made from membrane protein-to-lipid ratios 1:100, 1:10, and 1:1 were 1.86-fold, 5.05-fold and 5.27-fold that of Lipo-DiD group respectively. On the contrary, the distribution of NM-Lipo-DiD (1:10) in sham-operated brains was negligible and nonspecific (Fig. S10a and b), confirming the inflammation tropism of NM-Lipo. 12 h post injection, the fluorescent signals of biomimetic groups were attenuated by 9%~22% that of the initial level compared with 35% in the Lipo-DiD group, indicating prolonged accumulation at the ischemic lesion. Interestingly, the fluorescent intensity of spleens in the NM-Lipo-DiD (1:10) and NM-Lipo-DiD (1:1) group was reduced to 45% and 37% that of Lipo-DiD respectively due to the immune evasion effects of NM which avoid the clearance of NPs from the reticuloendothelial system (RES) (Fig. 4f and g) [21].

Collectively, neutrophil membrane camouflage greatly enhanced the

targeting capability of the nanoparticles to the ischemic brain, and the homing mechanism was mediated with the membrane protein interaction between NM and inflamed BBB and abundant chemokines at the lesion site [33]. NM-Lipo at a medium membrane protein-to-lipid ratio of 1:10 was witnessed with a potent targeting ability comparable to that of 1:1, and thus can be utilized for targeted stroke treatment *in vivo*.

2.5. *In vivo therapeutic effects on ischemic stroke*

Based on the outcomes of targeting ability, membrane protein-to-lipid ratios of 0:1, 1:100, and 1:10 were chosen to elucidate the impact of cell membrane cloaking on IS management and were denoted as Leo@Lipo, Leo@NM-Lipo L, and Leo@NM-Lipo H respectively. The design of animal experiments was shown in Fig. 5a and the therapeutic effects on ischemic stroke were assessed using the tMCAO rat model. The brain slices were
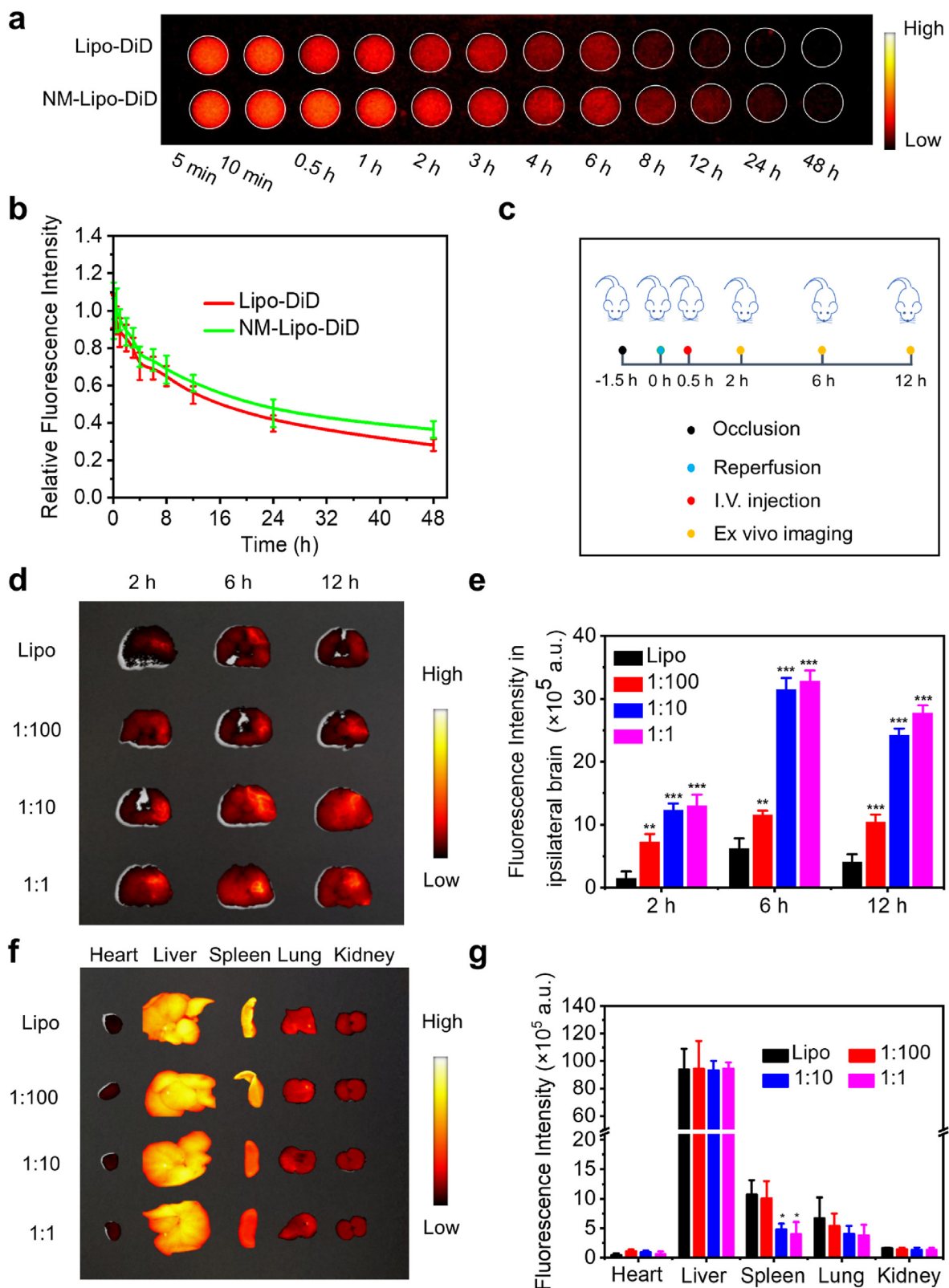
Fig. 4. Long plasma retention and preferential targeting to the inflamed lesion. **(a)** Image of plasma collected from healthy rats injected with Lipo-DiD and NM-Lipo-DiD. **(b)** Blood retention profile of Lipo-DiD and NM-Lipo-DiD after a single intravenous injection calculated by the ratio to the initial fluorescence intensity measured by a microplate reader. **(c)** Illustration of experimental design for ex vivo imaging studies. **(d)** Ex vivo imaging of DiD-labeled Lipo, NM-Lipo 1:100, NM-Lipo 1:10, and NM-Lipo 1:1 in the brain of tMCAO rats 2 h, 6 h, 12 h postinjection. **(e)** Quantification of the corresponding fluorescence intensity. **(f)** Ex vivo fluorescent images of major organs from tMCAO rats 6 h after injection of DiD-labeled Lipo, NM-Lipo 1:100, NM-Lipo 1:10, and NM-Lipo 1:1. **(g)** Quantitative analysis of the corresponding fluorescence intensity. Data represent mean ± SD, n = 6. Variance among groups was determined by one-way ANOVA with Tukey multiple comparisons post-hoc test. $*p < 0.05$, $**p < 0.01$, $***p < 0.001$.
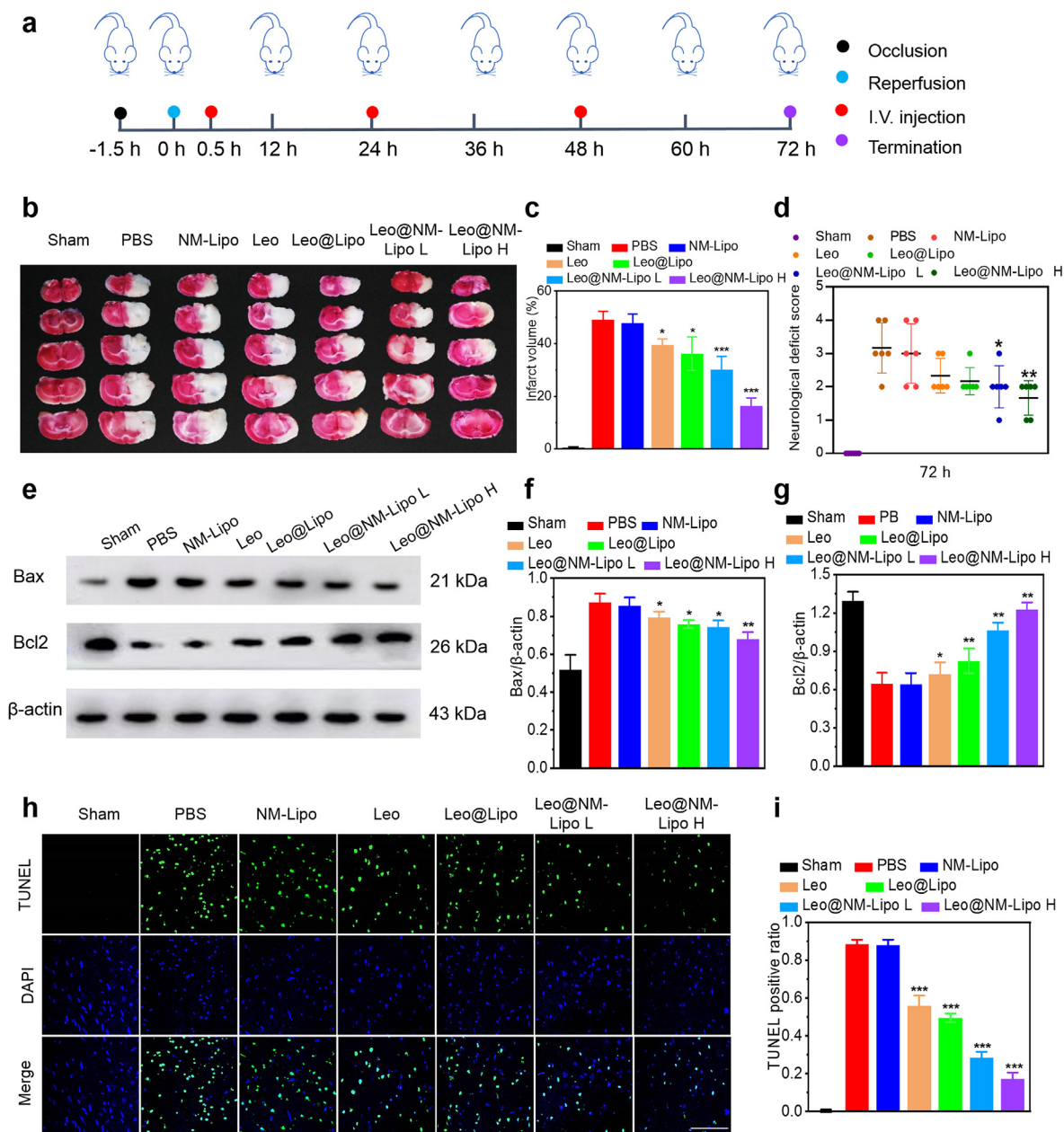
Fig. 5. Leo@NM-Lipo reduced infarct volume and neuron loss after ischemia-reperfusion (I/R) insult. **(a)** Scheme of the *in vivo* study design. Animals were sacrificed 3 days after tMCAO surgery. **(b)** Representative images of TTC-stained brain slices. **(c)** Quantification of infarct volume 72 h after reperfusion in tMCAO rats of different groups by ImageJ. **(d)** Neurological deficit scores 72 h postinjection in different groups. **(e)** Western blot of apoptosis-associated protein expression. The corresponding quantification of **(f)** Bax and **(g)** Bcl2 was analyzed by ImageJ. **(h)** Representative images of TUNEL staining in ischemic penumbra after different treatments (green; blue: DAPI, scale bar = 100 μm). **(i)** Quantitative analysis of TUNEL positive ratio by ImageJ. Data represent mean ± SD, n = 6. Variance among groups was determined by one-way ANOVA with Tukey multiple comparisons post-hoc test. *$p < 0.05$, **$p < 0.01$, ***$p < 0.001$.

stained with 2, 3, 5-triphenyltetrazolium chloride (TTC) 72 h post reperfusion (Fig. 5b). An evident infarct volume of 49.28% was observed in PBS treated model group, and NM-Lipo shared similar results while Leo and Leo-loaded nanotherapeutics treated groups all exhibited significant decreases in the size of infarct core. Strikingly, Leo@NM-Lipo H reduced the cerebral infarction volume to as low as 16.48%, which was 33.4%, 41.6%, 45.4%, and 54.4% that of the model, NM-Lipo, free Leo, and Leo@NM-Lipo L group respectively (Fig. 5c). Besides, the neurological scores of the rats were recorded 24, 48, and 72 h after reperfusion (Fig. S11a and b, and Fig. 5d). We found that both of Leo@NM-Lipo L and H groups significantly ameliorated neurological deficit 72 h post reperfusion compared with the model group, suggesting potent

neuroprotective effects, probably due to enhanced lesion-targeting delivery mediated by NM coating (Fig. 5d).

Neurons are extremely sensitive to oxygen and glucose deficiency. Therefore, they are susceptible to ischemic injuries and die in large numbers within hours of ischemia. The Bcl2 gene family plays an important role in regulating apoptosis after brain injury. WB analysis of the ischemic brain tissues demonstrated that the expression level of Bcl2 (anti-apoptotic protein) was tremendously elevated while that of Bax (apoptosis promoting protein) was reduced upon Leo and Leo-loaded nanoagents treatments in comparison with PBS or NM-Lipo group (Fig. 5e–g). In addition, the TUNEL assay was also employed to detect the apoptosis of cortical neurons in rats. The results showed that the number

of apoptotic cells of the Leo@NM-Lipo H group notably declined to 19.7% that of the PBS group and 31.1%, 35.1%, and 60.7% that of Leo, Leo@Lipo, and Leo@NM-Lipo L groups respectively (Fig. 5h and i). Overall, the therapeutic effects of Leo-loaded nanotherapeutics were positively correlated to the NM proportion in the formulation and Leo@NM-Lipo H exerted the most potent neuroprotective effects.

To disclose the underlying mechanism of the neuroprotective effects of Leo@NM-Lipo, we first investigate the anti-oxidant performance. The brain tissue sections were immunostained with 8-hydroxyguanosine (8-OHG), a sensitive oxidative stress biomarker, which was increased in tMCAO rats (Fig. 6a and b), in line with significant elevation of ROS level (Fig. S12). Moreover, the concentration of lipid peroxidation product malondialdehyde (MDA) and antioxidant superoxide dismutase (SOD) were assessed in the homogenate of ischemic brain tissues. Compared with the PBS group, ROS and MDA levels in tMCAO rats declined whereas SOD level was elevated to different degrees after treatment with Leo-containing formulations. Notably, the ROS, MDA, and SOD level in the Leo@NM-Lipo H group was comparable to that of the sham group, which was 41.2%, 50.5%, and 173.8% that of model group, indicating significantly alleviated oxidative stress and strengthened anti-oxidant defense in the lesion site (Fig. S12-13).

Astrocytes and microglia are the main inflammatory cells and their activation leads to vigorous inflammatory response and glial scar formation, which eventually causes further brain damage [34]. Therefore, we detected the expression level of ionized calcium-binding adaptor-1 (Iba-1, a marker of microglia) and glial fibrillary acidic protein (GFAP, a marker of astrocytes) in the brain sections of tMCAO rats by immuno-histochemical staining. Compared with the sham group, the expression of Iba-1 and GFAP were noticeably elevated in brain sections of tMCAO rats, suggesting enhanced proliferation and activation of astrocytes and microglia in the lesion (Fig. 6c–e). After treatment with Leo or Leo-loaded nanoparticles for 3 days, the number of Iba-1 and GFAP positive cells was significantly reduced, ranging from 45.3–85.2% and 28.2–69.9% that of the PBS group respectively.

Cytokines are key players in neuroinflammation and are secreted from different cells in the brain including microglia, astrocytes, endothelial cells, neurons, and infiltrated leukocytes [35]. Pro-inflammatory cytokines including TNF-α, IL-1β, and IL-6 can aggravate cerebral ischemia-reperfusion injury while anti-inflammatory factors such as IL-10 and TGF-β and neurotrophic factors can promote tissue repair and neuron regeneration [36]. In our study, drastically enhanced secretions of proinflammatory cytokines TNF-α and IL-1β were observed in tMCAO rats' brain tissue compared with the sham group (Fig. 6f and g), which significantly declined after different Leo formulation treatments. Interestingly, NM-Lipo alone decreased the TNF-α and IL-1β levels by 10.7% and 15.8% of the PBS group respectively, probably due to the potent inflammation-neutralizing ability of NM coating. Moreover, Leo@NM-Lipo L and H group further decreased the TNF-α and IL-1β expressions to 19.2% and 26.2% that of the PBS group. As manifested in Fig. 6h, IL-10 expression was significantly elevated after Leo, Leo@Lipo, Leo@NM-Lipo L, and H treatments, which are 1.2-fold, 1.3-fold, 1.5-fold, and 1.7-fold that of the model group respectively. Remarkably, the Leo@NM-Lipo H group showed the lowest level of TNF-α and IL-1β but the highest level of IL-10, suggesting remodeled proinflammatory immune microenvironment to favor neuroprotection.

BBB plays a pivotal role in the maintenance of central nervous system (CNS) homeostasis and neuronal function. It is disrupted in the early stage of IS, allows the swarming of detrimental factors into the brain parenchyma, and consequently aggravates neuroinflammation and neurodegeneration [37]. Hypoxia-inducible factor-1 alpha (HIF-1α) is a sensitive regulator of oxygen homeostasis and plays divergent roles in the pathophysiology of IS, which is sophisticatedly regulated by the spatio-temporal expression [38]. Recent studies showed that elevated HIF-1α level compromised BBB integrity in the acute phase of IS through tight junctions (TJs) alterations in hypoxic conditions [39–41]. Consistent with previous reports, significantly elevated expression of HIF-1α was

observed in tMCAO rats after 72 h reperfusion, which was 2-fold that of the sham group (Fig. 7a, b). On the contrary, after treatments with different Leo formulations, the HIF-1α expression level declined to 65.2%–82.8% that of the model group. In parallel, key TJs proteins including Occludin and claudin-5 dramatically declined in the tMCAO model compared to the sham group whereas Leo and Leo-loaded nano-therapeutics substantially suppressed the degradation of TJs to alleviate BBB damage (Fig. 7a, c, d). Furthermore, we demonstrated that EB leakage in the ipsilateral hemisphere of Leo, Leo@Lipo, Leo@NM-Lipo L, and H groups was diminished to 43.4%, 36.4%, 31.2%, and 18.81% that of the model group, indicating significantly ameliorated BBB integrity (Fig. 7e and f).

### 2.6. In vivo biosafety evaluations

To evaluate the preliminary safety *in vivo*, potential side effects were investigated in tMCAO rats after treatment with nanoformulations at an equivalent dosage of Leo at 10 mg kg^{-1} day^{-1} for 3 days. The body weights of tMCAO rats after different treatments were closer to the healthy rats compared with the PBS group (Fig. S14). Serological biochemistry results manifested that biochemical markers including alanine Aminotransferase (ALT), aspartate aminotransferase (AST), blood urea nitrogen (BUN), and creatinine (CRE) levels were comparable to that of the sham group, indicating well-preserved liver and kidney functions (Fig. S15). Subsequently, hematoxylin-eosin (HE) stained sections of major organs including the heart, liver, spleen, lung, and kidney showed no evidence of abnormality or inflammatory cells infiltration (Fig. S16). The HE staining of brain sections showed sparse structure and massive necrosis in the ischemic hemispheres of tMCAO rats, while Leo@NM-Lipo group displayed well-preserved cerebral tissues comparable to that of sham group (Fig. S17). Meanwhile, the contralateral hemispheres of all the groups showed no abnormality or inflammatory cell infiltration, indicating that the nanosystems constructed in this study had good biocompatibility in the brain. Collectively, the biomimetic nanoplatform demonstrated negligible systemic toxicity and good biosafety.

3. Discussion

Ischemic stroke (IS) constitutes the second leading cause of mortality and morbidity and has inflicted a considerable socio-economic burden on the health system worldwide [42]. Nowadays, the combination of vascular recanalization and neuroprotection is a well-established paradigm for the treatment of IS, the former to restore blood flow while the latter to alleviate I/R injury [43]. Despite that a variety of nanoplatforms including polymer nanoparticles, amphiphilic polymer micelles, and inorganic nanoparticles have emerged to enhance drug delivery efficiency for IS treatment [44], many neuroprotectants including Leo so far have failed to be formulated into nanomedicine due to poor solubility both in water and organic solvents.

Liposomes are sphere-shaped vesicles composed of phospholipid bilayers, which have been widely investigated to encapsulate a great diversity of therapeutic payloads for the treatment of cancer, infections, *etc.* [45,46]. Currently, around 20 liposomal drugs have been applied in clinics so far, including COVID-19 mRNA vaccines [45,46]. Therefore, liposomes represent ideal nanocarriers for neuroprotectants delivery due to their potent drug-loading capacity and clinical application potential. In this work, nanoliposomes with a specific molar ratio of phospholipid composition (DPPC: DSPE-mPEG-2000: cholesterol = 20: 1: 10) were yielded by the thin film evaporation and extrusion through polycarbonate membranes. Subsequently, Leo with typical pH-dependent solubility (~30-fold decrease from pH 4.0 to pH 7.4) was loaded into the aqueous core by the pH gradient method before further functionalization.

Advancements in cell membrane coating technology provide a one-step strategy for nanoparticle functionalization with multiple merits
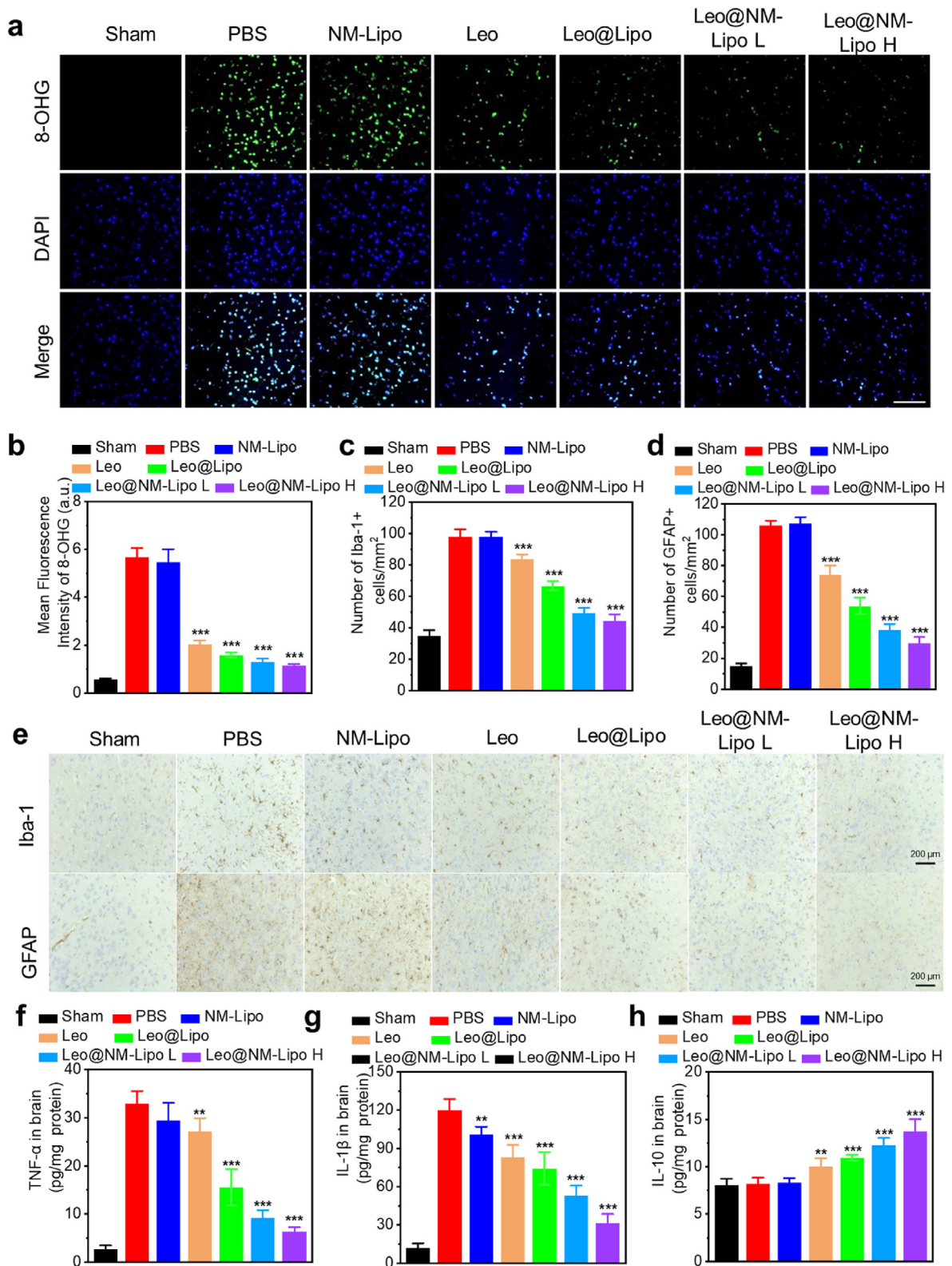
Fig. 6. Oxidative stress alleviation and Inflammation resolution in the ischemic brain. **(a)** Immunofluorescent staining of oxidative stress (green: 8-OHG; blue: DAPI) in the ischemic penumbra in different groups (scale bar = 100 μm). **(b)** Corresponding quantitative analysis of fluorescence intensity by ImageJ. The number of **(c)** Iba-1 positive and **(d)** GFAP positive cells in the corresponding brain sections were quantified by ImageJ. **(e)** Iba-1 and GFAP expression in the ipsilateral brain sections of rats after different treatments were examined by immunohistochemical staining (Scale bar = 200 μm). Expression levels of **(f)** TNF-α, **(g)** IL-1β, and **(h)** IL-10 in the ipsilateral hemisphere after different treatments were measured by the Elisa test. Data are expressed as mean ± SD, n = 6. Variance among groups was determined by one-way ANOVA with Tukey multiple comparisons post-hoc test. *$p < 0.05$, **$p < 0.01$, ***$p < 0.001$.
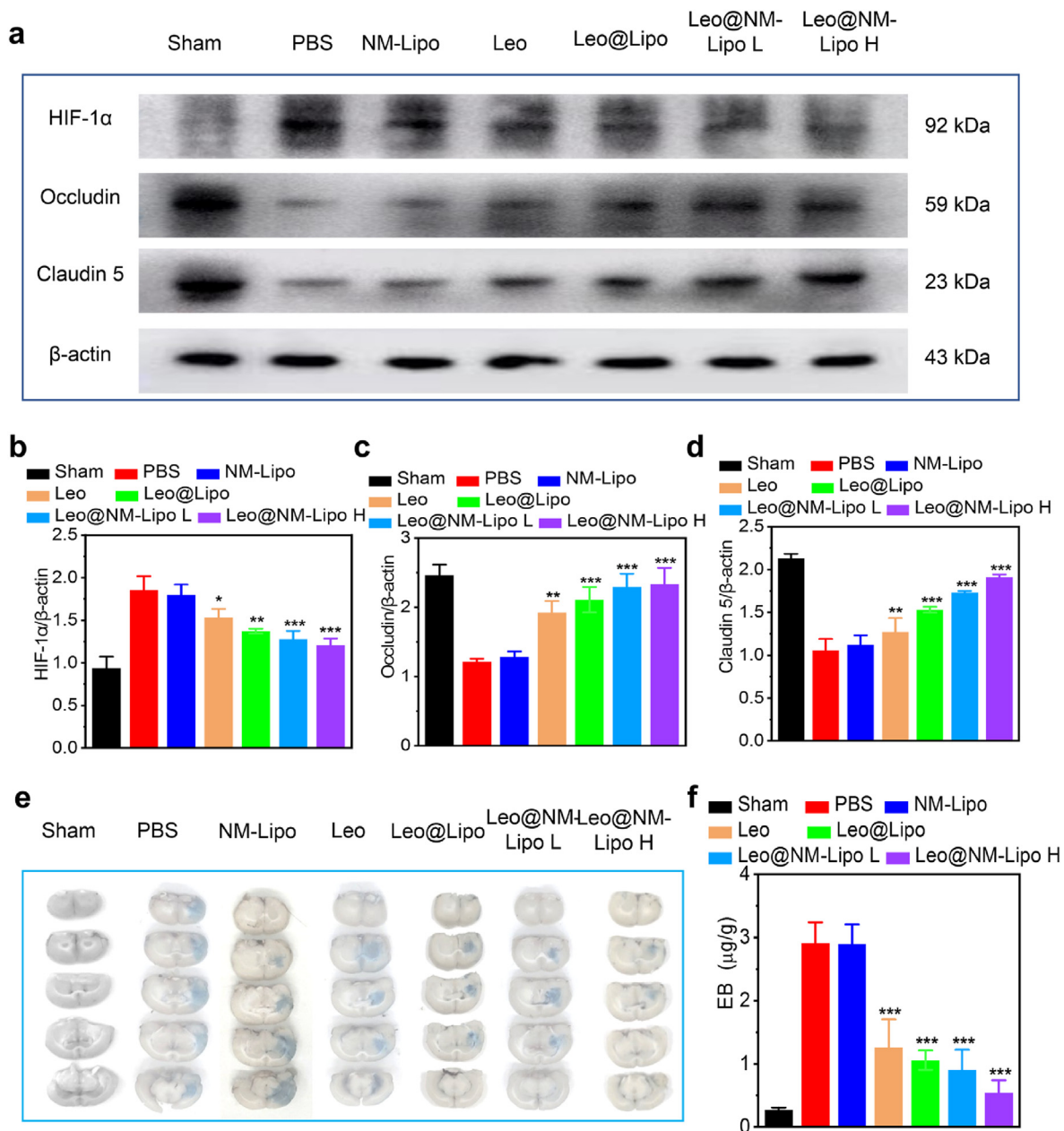
Fig. 7. Leo@NM-Lipo alleviated BBB disruption induced by ischemia-reperfusion (I/R) injury. **(a)** Western blot of hypoxia-associated protein (HIF-1α) and BBB tight junction-related protein expression after treatment with various formulations. Corresponding quantification of protein expression levels of **(b)** HIF-1α, **(c)** Occludin, and **(d)** Claudin 5 were processed by ImageJ. **(e)** Brain sections of rats injected with EB after I/R in different groups. **(f)** Quantitative analysis of EB dye leakage through the brain of rats by ImageJ. Data are presented as mean ± SD, n = 6. Variance among groups was determined by one-way ANOVA with Tukey multiple comparisons post-hoc test. $*p < 0.05$, $**p < 0.01$, $***p < 0.001$.

inherited from source cells. To date, a variety of cell membranes such as erythrocytes [47], platelet [48], leukocytes [18,49], stem cells [50], and even cancer cells [51] have been utilized for targeted IS therapy. Given their crucial roles in the pathogenesis of IS, neutrophils were selected as cell membrane donors due to the rapid lesion tropism and inflammation neutralization capability [20]. Generally, the neutrophil membrane can be derived either from natural neutrophils in human/animal peripheral blood [21,52] or HL-60 differentiated neutrophil-like cells [22,53]. As cell membranes possess complex biological and interfacial functionalities, scalable manufacturing needs to comply with economic fabrication processes. In this regard, differentiated HL-60 cells would be a more pragmatic choice as natural neutrophils cannot be subcultured and the sources are extremely limited (*e.g.* ∼ 2×10^7 neutrophil cells per mouse with neutrophilia) [54].

In our study, a combination of 10 ng mL^{-1} TNF-α with 1.25% DMSO was employed to differentiate HL-60 towards inflammation-activated neutrophils-mimetic cells [55]. Subsequently, Leo-loaded nano-liposomes (Leo@Lipo) were further co-extruded with NM to construct Leo@NM-Lipo. Successful membrane coating was validated by physico-chemical and SDS-PAGE characterizations (Fig. 1a–d) along with co-localization observation (Fig. S3). Besides, western blotting results confirmed the presence and enrichment of key neutrophil membrane proteins on Leo@NM-Lipo, including TNF-α receptors (TNF-αR), IL-1β receptors (IL-1βR), CD 11b, and LFA, PECAM-1 and Integrin β2 (Fig. 1e) [56]. Moreover, Leo@NM-Lipo with a high drug loading (13.5 wt%) and high encapsulation efficiency (78.51%) was obtained by optimizing the lipid-to-drug weight ratios (Fig. S4), which exhibited excellent storage stability in terms of size and drug content (Fig. 1f and g). Furthermore,

the drug release of Leo@NM-Lipo followed a first-order kinetic profile and the release mechanism was determined to be Fickian diffusion according to the Ritger-Peppas model fitting (n < 0.5) (Table S2).

To date, the weight ratios of cell membrane protein-to-nanocores generally varied from 2:1 to 1:300 for cell membrane-camouflaged nanoagents [57,58], and sometimes pure cell membrane nanovesicles were utilized for nanomedicine formulation [22]. Apparently, cell membrane-to-nanocore ratios directly impact the physicochemical properties including coating integrity, size distribution, and zeta potentials of the resulting nanosystems [25,51]. Nonetheless, their influence on the biological performance of cell membrane-cloaked nanoagents remains to be explored. To this end, we co-extruded NM and Leo@Lipo with membrane protein-to-lipid weight ratios. The as-obtained Leo@NM-Lipos exhibited no significant differences in sizes, which were well controlled by the pore size of polycarbonate membranes during extrusion. Besides, the zeta potentials of Leo@NM-Lipos varied between pure membrane vesicles and Leo@Lipo, suggesting successful membrane fusion (Fig. S5).

Subsequently, the inflammatory cytokines sequestering ability of Leo@NM-Lipos was assayed to explore the anti-inflammation potential (Fig. 2a and b). Overall, the binding ability of neutrophil-mimetic nanoliposomes was positively correlated with the proportion of NM. Surprisingly, the binding ability of Leo@NM-Lipo was much more potent than that of previously reported neutrophil membrane camouflaging nanoparticles (NM-NP) even at a much lower membrane coating ratio [21,24,52], probably due to superior membrane fusion efficiency as liposomes possessed the utmost similarity to the cell membranes. For example, the IC_{50} of NM-Lipo 1:10 was as low as ~100 μg mL^{-1} for both TNF-α and IL-1β, which were only 10%~50% that of NM-NP 1:1 cloaked by human [24] or rat [21] neutrophil membrane. Hence, Leo@NM-Lipo can bind inflammatory factors more efficiently that would otherwise act on endogenous neutrophils and other immune cells to intensify the inflammatory cascades. Moreover, the bold cytokines binding capability also verified right-side-out protein orientation on the nanosurface of Leo@NM-Lipo [24].

To investigate the anti-oxidant and BBB protective potential of Leo@NM-Lipo (at a fixed membrane protein-to-lipid ratio of 1:10), a transwell model with BCECs seeded in the upper chamber and PC12 cells in the lower chamber subjecting to OGD/R treatment was established to mimic I/R insult on neurons and BBB integrity at the same time (Fig. 2c–g). Regarding PC12 cells, Leo@NM-Lipo significantly reduced ROS production and enhanced the survival rate of PC12 in response to OGD/R exposure. Besides, Leo@NM-Lipo preserved the blood-brain barrier (BBB) integrity against OGD/R insult through TEER measurements, probably due to upregulated expression of tight junctions [12].

In terms of targetability, our results showed that a higher proportion of the neutrophil membrane led to superior targetability in the range of 1:1–1:500 in vitro (Fig. 3, S7), which was associated with upregulated expression of ICAM-1 and VCAM-1 in inflammatory brain microvascular endothelial cells (Fig. S6-9). Interestingly, 1:10 group showed significantly higher cellular uptake than those prepared with lower membrane ratios (0:1, 1:500, 1:100, 1:50, and 1:25) but not significantly lower than those prepared with higher membrane ratios (1:5 and 1:1) (Fig. S7). In parallel, there was no significant difference between 1:1 and 1:10 in tMCAO rats (Fig. 4). On the one hand, these results indicated that simply increasing the NM proportion not necessarily resulted in superior targeted delivery efficiency probably. On the other hand, it can be speculated that Leo@NM-Lipo only required a low amount of neutrophil membrane to exert its ischemic lesion targeting functions, which is of high interest from the perspective of large-scale production. Besides, the slightly prolonged plasma retention time of NM-Lipo over PEG-coated Lipo was attributed to cell membrane coating (Fig. 4a and b) [31]. Taken together, NM-Lipo replicated the targeting and immune evasion properties of natural neutrophils with low cell membrane proportion.

Encouragingly, Leo@NM-Lipo exhibited excellent therapeutic potential in the tMCAO rats (Fig. 5). After treatments for three days, Leo@NM-Lipo significantly reduced the infarct volume and neurological deficits induced by I/R injury compared with other groups (Fig. 5b–d). Moreover, Leo@NM-Lipo tremendously reduced neuron apoptosis as substantiated by the decreased number of TUNEL-positive cells, accompanied by upregulation of Bcl2 protein and downregulation of Bax protein (Fig. 5e–i). Afterward, further investigations over major pathological characteristics and therapeutic targets including oxidative stress, neuroinflammation, and BBB dysfunction were executed to disclose the underlying mechanisms.

Oxidative stress is a key cause of I/R insult and an initiator of neuronal dysfunction and death, mainly through the overproduction of peroxides and depletion of antioxidants. In our study, Leo@NM-Lipo significantly alleviated oxidative stress (Fig. 6a and b) by scavenging ROS (Fig. S12) and inhibiting lipid peroxidation while increasing antioxidant enzyme SOD expression (Fig. S13). Remarkably, the oxidative stress level in the NM-Lipo was comparable to that of the model group, indicating that the antioxidant property of Leo@NM-Lipo was derived solely from Leo [11,59]. Nonetheless, Leo@NM-Lipo H obtained the most robust antioxidant effects compared with Leo@NM-Lipo L, suggesting NM-mediated lesion targeting is a substantial contributor to boosting the therapeutic efficacy of free Leo.

Inflammation is another major target for therapeutic interventions of IS [35]. The first resident immune cells to respond are microglia, which migrate to both the infarct core and penumbra regions and release detrimental factors including proinflammatory cytokines, ROS, and chemokines, resulting in the additional chemoattraction of circulating leukocytes. Astrocytes are another key players in I/R injury, which contribute to the synthesis of inflammatory factors such as monocyte chemotactic protein-1, IL-1β, glial and fibrillary acidic protein (GFAP) that can lead to reactive gliosis and later scar formation. In our studies, Leo@NM-Lipo H not only inhibited the recruitment of astrocytes and microglia during I/R insult (Fig. 6c–e) but also reversed the hostile inflammatory microenvironment to favor neuroregeneration, which was validated by significantly declined proinflammatory cytokines and elevated anti-inflammatory cytokine (Fig. 6f–h). Besides, the consolidated anti-inflammation effects of Leo@NM-Lipo with higher NM proportion could be attributed to enhanced drug accumulation in the lesion and synergistic anti-inflammation efficacy originating from inflammation cytokines binding. Interestingly, NM-Lipo also achieved inflammation downregulation to some extent yet it alone failed to combat I/R injury, probably due to the complexity and heterogeneity of the cerebral microenvironment [60].

BBB integrity is crucial for the homeostasis of the CNS and accumulating evidence implicated that BBB damage is both the result and the cause of I/R insult [61]. The tight junctions (TJs) between the endothelial cells serve to restrict blood-borne substances from entering the brain. Decreased TJs integrity results in increased paracellular permeability, directly contributing to cerebral vasogenic edema, hemorrhagic transformation, and poor prognosis. Meanwhile, ischemia results in profound tissue hypoxia and microvascular dysfunction. Hypoxia-inducible factor-1α (HIF-1α) is considered a pivotal regulator of oxygen homeostasis and is strictly regulated by oxygen levels. Under the hypoxic condition, HIF-1α signals upregulate the expression of MMP-9 and vascular endothelial growth factor (VEGF), subsequently leading to TJs degradation [62,63]. Therefore, HIF-1α played a detrimental role in BBB impairment. Our results demonstrated that administration with Leo@NM-Lipo for three consecutive days resulted in significantly reduced HIF-1α levels together with more pronounced TJs expressions and attenuated EB leakage in the ischemic brain (Fig. 7). Hence, Leo@NM-Lipo constitutes a new therapeutic approach to combat BBB dysfunction.

Last but not the least, this biomimetic liposome drug delivery system

was proven with excellent biocompatibility both *in vitro* (Fig. 2h–j) and *in vivo* (Fig. S16). Leo@NM-Lipo demonstrated desirable hemocompatibility, which can be particularly advantageous in treating vascular disorders. Leo@NM-Lipo exhibited negligible toxicity *in vitro* with BCECs and PC12 cells below 2 mg mL-1 (Fig. 2i, j). Furthermore, Besides, *in vivo* studies further confirmed its biosafety with well-preserved liver and kidney functions and the absence of pathological changes in the HE-stained sections of major organs including the heart, liver, spleen, lung, kidney (Fig. S16) and brain (Fig. S17).

Collectively, Leo@NM-Lipo represents a potent nanomedicine candidate for targeted brain salvage against I/R injury. Owing to the dynamic functions of the neutrophil membrane proteins, a simple, safe, and multifunctional nanosystem integrating accurate lesion-targeting and boosted therapeutic efficacy was successfully established through rational optimization, bypassing the necessity of sophisticated chemical modifications. Moreover, a series of quality control and therapeutic effects verifications were executed to ensure the safety, reproducibility, and efficacy of Leo@NM-Lipo for IS management. Furthermore, the as-established neutrophil-mimetic platform holds extensive clinical prospects considering the broad application potentials of neutrophil-inspired drug delivery systems for the treatment of ischemic stroke [21], myocardial infarction [52], cancer [64], arthritis [65], acute pancreatitis [66], infections [54], *etc.*

4. Conclusions

To summarize, we successfully constructed a biomimetic nanoplatform composed of neutrophil membrane-camouflaged nanoliposomal leonurine (Leo@NM-Lipo), which exhibited high drug loading efficiency, sustained drug release, and excellent storage stability while inheriting the inflammation chemotaxis, inflammatory cytokines sequestration and immune evasion from natural neutrophils. Consequently, this strategy assured the enrichment and sustained release of Leo across BBB to the infarct core to suppress apoptosis, attenuate oxidative stress and counteract neuroinflammation which in turn significantly relieved ischemic damage and ameliorated neurological functions. Notably, our systematic investigations demonstrated that the biomimetic nanoliposomal platform only required a low amount of neutrophil membrane (~10% of the weight of the nanoliposomes) to exert its natural function both at the cellular and animal level. Hence, this neutrophil-mimetic strategy achieving multi-targeting and multi-level modulation confers a perspective to promote the bench-to-bed translation of drug therapy for a wide spectrum of inflammatory diseases including cerebral disorders.

5. Materials and methods

5.1. Materials

Detailed information was listed in supplementary materials.

5.2. Cells and animals

Human HL-60 cells (Human promyelocytic leukemia cell) and PC12 cells (Neuron-like rat pheochromocytoma cell line) were obtained from the Cell Bank of the Chinese Academy of Sciences. HL-60 cells were cultured in IMDM containing 20% FBS, 1% penicillin/streptomycin, and PC12 cells were cultured in RPMI 1640 medium supplemented with 10% horse serum, 5% FBS, 1% penicillin/streptomycin. BCECs (Rat brain capillary endothelial cells) were purchased from Procell Life Science & Technology (Wuhan, China). BCECs were cultured in DMEM supplemented with 10% FBS, and 1% penicillin/streptomycin. All the cells were cultured at 37 °C in a humidified atmosphere with 5% CO_2.

SPF-grade Male Sprague Dawley (SD) rats (250–280 g) were purchased from SPF Biotechnology Co., Ltd, Beijing, China. The rats were housed at 12 h light/dark cycle with access to water ad libitum and a standard laboratory diet. All the animal study protocols were approved by the Ethics Committee of the Animal Center of Macau University of Science and Technology.

5.3. Derivation of neutrophil membranes (NM)

HL-60 cells were cultured in IMDM with 20% FBS and 1% penicillin/streptomycin. To obtain inflammation-activated neutrophil-like cells, HL-60 cells were differentiated with DMSO (1.25 vol%) and TNF-α (10 ng mL^{-1}) for 4 days [53]. After rinsing with $1 \times$ PBS and centrifuged 3 times at 800 rpm for 10 min, differentiated HL-60 cells were resuspended in IB-1 solution (225 mM mannitol, 75 mM sucrose, 30 mM Tris-HCl, 0.5 mM EDTA, 0.5% BSA) and disrupted with a Dounce homogenizer for 50 times and centrifuged at 20,000 g for 30 min at 4 °C. Subsequently the supernatant was centrifuged at 100,000 g for 60 min at 4 °C. Finally, membranes were collected and carefully washed twice with 0.2 mM EDTA and stored at − 80 °C for further studies.

5.4. Identification of differentiated neutrophils

Neutrophil-specific membrane proteins on differentiated and undifferentiated HL-60 cells were examined by western blotting. In brief, samples were lysed using RIPA lysis buffer containing protease inhibitor cocktail, and the lysates were centrifuged (12,000 g, 5 min, 4 °C). The total protein contents of supernatants were quantified by enhanced BCA protein assay and then mixed with loading buffer. Next, an equivalent 20 μg protein of each sample was loaded into each well of Tris/glycine SDS-polyacrylamide gel and separated by electrophoresis. Afterward, the proteins were transferred to PVDF membranes and then blocked with TBST containing 5% non-fat milk powder for 1 h at room temperature. The PVDF membranes were incubated with the corresponding primary antibodies against CD11a, CD11b, PECAM-1, Integrin β2, and GAPDH overnight at 4 °C. Then, the PVDF membranes were washed by TBST and then incubated with horseradish peroxidase (HRP)-conjugated secondary goat anti-rabbit IgG antibody for 1 h at room temperature. Finally, protein bands were visualized and analyzed by ImageJ software. Nuclear morphologic changes of HL-60 cells were observed by Giemsa staining.

5.5. Preparation of Lipo, NM-Lipo, and Leo@NM-Lipo

DPPC, DSPE-PEG2000, and cholesterol were dissolved in chloroform with a molar ratio of 20:1:10 and evaporated through a rotary evaporator to form a thin film. Afterward, the film was hydrated with saline or citrate solution (pH = 4.0) and homogenized with ultrasound for 5 min. Next, lipid suspension was extruded 15 times through 400, 200, and 100 nm polycarbonate membranes to assemble nanoliposomes (Lipo). To obtain Leo@Lipo, leonurine (Leo) was added to Lipo suspension at different weight ratios (1:5, 1:10, and 1:20) and sodium bicarbonate was used to adjust the pH value of the suspension to 7.0 to generate pH gradient which drives Leo encapsulation into the aqueous core of Lipo. To obtain Leo@NM-Lipo, Leo@Lipo was vortexed with NM suspension and extruded through a polycarbonate membrane using Avanti® mini extruder. Afterward, the nanoliposomes were purified with fresh PBS 5 times by centrifugation with centrifugal filter units (Millipore, MA, USA) at 5000 g for 15 min.

The membrane protein was quantified using BCA protein assay kit. For NM camouflage, blank Lipo or Leo@Lipo was mixed with NM suspension at membrane protein-to-lipid weight ratios of 0:1, 1:1, 1:10, 1:100, 1:500, and vortexed for 5 min. Then the mixture was extruded through a polycarbonate membrane with different pore sizes (from 800 nm to 200 nm) using Avanti® mini extruder to facilitate the fusion of NM with liposomal bilayers. For fluorescence labeling, fluorescent dye DiD was mixed with the lipids at a weight ratio of 1:1000 during thin film evaporation. To label NM, another fluorescent dye DiO was mixed with NM at a weight ratio of 1:1000, followed by sonication for 3 min and incubation for 10 min on ice. Free dyes were removed by centrifugation.

5.6. Characterizations of nanoliposomes

The morphology of nanosystems was visualized with a transmission electron microscope (TEM) (JEM-2100, JEOL, Japan) after staining with a drop of 1% phosphotungstic acid solution. The hydrodynamic size and zeta potential of nanoliposomes were characterized by Zetasizer Nano ZS (Malvern, UK) at 25 °C. The characteristic membrane proteins of Lipo, NM, and NM-Lipo were identified by western blot as previously described except that the primary antibodies of LFA-1, CD11b, PECAM-1, Integrin β2, IL-1R, and TNF-αR were used. Meanwhile, the surface protein expression profile of nanoparticles was detected by gel electrophoresis and Coomassie blue staining.

To evaluate the drug loading capacity of Leo@NM-Lipo, supernatant after each centrifugation was collected to detect free Leo by UV spectrophotometry (UV-2450, Shimadzu, Japan) at 277 nm. The drug loading (DL) and encapsulation efficiency (EE) of Leo-loaded nanoliposomes was calculated according to the following equation:

$$DL\ (\%) = \frac{Weight\ of\ total\ Leo - Weight\ of\ free\ Leo}{Weight\ of\ nanoparticles} \times 100\% \quad (1)$$

$$EE\ (\%) = \frac{Weight\ of\ total\ Leo - Weight\ of\ free\ Leo}{Weight\ of\ total\ Leo} \times 100\% \quad (2)$$

The dispersion stability of nanoliposomes at 4 °C was evaluated by measurement of hydrodynamic size with DLS for 15 days. Moreover, the leakage rate of Leo@NM-Lipo was studied using centrifugal filter units. At the given time points, Leo@NM-Lipo stored at 37 °C, 4 °C, and room temperature was centrifuged to remove free Leo, which was determined by UV spectrophotometry as described above.

$$Leakage\ rate\ (\%) = \frac{M_f}{M_0} \times 100\% \quad (3)$$

where M_f was the amount of free Leo leaked from the nanoliposomes and M_0 was the total amount of Leo initially encapsulated in the nanoliposomes.

5.7. Drug release kinetics in vitro

The drug release profiles of Leo@Lipo and Leo@NM-Lipo were studied using dialysis bags (MWCO 12–14 kDa, Spectrum™ Labs Spectra/Por™) [67]. 1 mL of Leo@Lipo and Leo@NM-Lipo were placed in dialysis bags, immersed in 50 mL of PBS (10 mM, pH 7.4) and shaken at 100 rpm at 37 °C. At predetermined time points, 1 mL of medium was collected and replenished with the same volume of fresh PBS. The concentration of Leo was determined by UV spectrophotometry and the cumulative release rate was calculated by the following equations:

$$Cumulative\ release\ (\%) = \frac{M_t}{M_0} \times 100\% \quad (4)$$

where M_t was the amount of drug released at predetermined time points and M_0 was the total amount of drug initially encapsulated in the nanoliposomes.

5.8. Inflammation neutralization capability of Leo@NM-Lipo in vitro

Leo@NM-Lipo prepared at different membrane protein-to-lipid weight ratios (0:1, 1:1, 1:10, 1:100, 1:500) was diluted to the final concentration of 32, 64, 128, 256, 512, 1024, 2048, 4096 μg mL^{-1} and mixed with 8 ng mL^{-1} rat TNF-α and IL-1β respectively. After incubation at 37 °C for 1 h, the mixtures were centrifuged at 12,000 rpm for 50 min at 4 °C to remove the nanoparticles and the residual TNF-α or IL-1β in the supernatant was quantified by enzyme-linked immunosorbent assay (ELISA) kit.

5.9. Oxygen-glucose deprivation/reoxygenation (OGD/R) model

OGD/R model was established as previously reported [68]. BCECs were seeded to the transwell inserts with 3 μm pore polycarbonate membrane (Corning Costar, Cambridge, MA, USA) and cultured until the trans epithelial electric resistance (TEER) exceeds 300 Ω cm^2 while PC12 cells were seeded in the lower chamber. PC12 cells and BCECs were further cultured with glucose-free medium and incubated with Leo, Leo@Lipo, or Leo@NM-Lipo (at an equivalent Leo concentration of 10 μM) under 94% N$_2$, 1% O$_2$, and 5% CO$_2$ for 6 h before reoxygenation to normal culture conditions for 2 h. Subsequently, 50 μL of CCK-8 was added to 450 μL medium in each well and incubated for 3 h at 37 °C. The absorbance was measured at 450 nm by a microplate reader to calculate the cell viability of PC12 cells. The TEER of BCECs was monitored by a cell resistance meter (Millicell-ERS, USA) for 24 h. To evaluate ROS levels, PC12 cells were treated with DCFHDA after reoxygenation for 2 h. The samples were photographed by a confocal microscope (Leica TCS SP8, Germany).

5.10. Cytotoxicity and hemolysis assay in vitro

BCECs and PC12 cells were cultured in 96-well plates at a density of 5 × 10^3 per well and incubated with Leo@NM-Lipo at different concentrations (1, 10, 20, 50, 100, 200, 400, 600, 800, 1000, and 2000 μg mL^{-1}) at 37 °C for 24 h. Afterward, each well was rinsed with PBS, replenished with 90 μL of free medium and 10 μL of CCK-8, and incubated for another 4 h at 37 °C. The absorbance of each well was measured at 450 nm by a microplate reader (SpectraMax ID5, Molecule devices, USA).

To study the hemocompatibility, fresh rat whole blood was collected to prepare a 4% RBC (red blood cell) suspension. Afterward, 200 μL Leo@NM-Lipo was added to 200 μL 4% RBC suspension to achieve a final concentration of 10, 20, 50, 100, 200, 500, and 1000 μg mL^{-1}. In parallel, 200 μL of distilled water and PBS were added into 200 μL of 4% RBC sample and served as negative and positive controls, respectively. All the samples were incubated at 37 °C for 3 h and centrifuged at 1500 rpm for 10 min. Finally, the absorbance of the supernatant at 540 nm was measured by a microplate reader and the hemolysis rate was calculated by the following equation:

$$Hemolysis\ (\%) = \frac{A_{sample} - A_{negative}}{A_{positive} - A_{negative}} \times 100\% \quad (5)$$

5.11. In vitro binding and penetrating ability across BBB

To evaluate the binding ability of nanoliposomes to inflamed BBB, BCECs monolayer was seeded in a confocal dish and cultured in medium with or without 10 ng mL^{-1} TNF-α for 6 h. Next, Lipo-DiD or NM-Lipo-DiD with various membrane protein-to-lipid ratios were added respectively. Cells without treatment were used as control. After incubation for 2 h, BCECs were washed, fixed with 4% PFA for 10 min and stained with DAPI for photographing by a confocal microscope (Leica TCS SP8, Germany). To validate NM-mediated cellular uptake, VCAM-1 and ICAM-1 expression on BCECs with or without TNF-α treatment were evaluated by western blotting.

The *in vitro* BBB penetrating capability of NM-Lipo was evaluated in a 24-well transwell plate. More specifically, BCECs were seeded in a donor chamber at a density of 1 × 10^5 cells/well, and the transendothelial electrical resistance (TEER) was monitored using a cell resistance meter (Millicell-ERS2, USA). When the TEER reached 300 Ω cm^2, the PC12 cells were seeded 2 × 10^5 cells/well on a glass slice in the bottom chamber. Before transmigration assays, the BCECs monolayer was pre-stimulated with 10 ng mL^{-1} TNF-α for 6 h. Meanwhile, NM-Lipo-DiD containing different membrane protein-to-lipid weight ratios (0:1, 1:1, 1:10, 1:100, 1:500) or Lipo-DiD or NM-Lipo-DiD (membrane protein-to-lipid weight ratio 1:10) were added in the upper chamber respectively. 3 h later, PC12 cells were washed, fixed with 4% PFA for 10 min, and stained with

DAPI for photographing by a confocal microscope (Leica TCS SP8, Germany). Cells without treatment were used as control. Quantification of NM-Lipo-DiD uptake in BCECs and PC12 cells was also measured respectively by flow cytometry (BD, USA).

5.12. Pharmacokinetic study

Healthy SD rats were intravenously injected with Lipo-DiD and NM-Lipo-DiD (equivalent DiD dose at 0.1 mg kg^{-1}). At predetermined time points (5 min, 10 min, 30 min, 1 h, 2 h, 3 h, 4 h, 6 h, 8 h, 12 h, 24 h, and 48 h), blood samples were collected and diluted with PBS in 96-well plates. Then, the fluorescence photograph was measured by an *in vivo* imaging system (FX Pro, Bruker, Germany), and the fluorescence intensity was measured by a microplate reader ($\lambda_{excitation/emission} = 644/665$ nm).

5.13. Establishment of transient middle cerebral artery occlusion (tMCAO) model

The tMCAO model was established by a suture-occluded method in rats [69]. Briefly, male Sprague-Dawley rats (250–300 g) were anesthetized with 4% pentobarbital sodium and placed on a heating pad in the supine position. The common carotid artery (CCA) was exposed through a midline incision in the neck and the external carotid artery (ECA) and the internal carotid artery (ICA) were separated. The silicon suture (Cinongtech, China) was then introduced from ECA into the ICA to occlude the blood supply of the middle cerebral artery. The rat was kept in a heated cage for 1.5 h and then the suture was removed to allow reperfusion for 0.5 h. Subsequently, PBS, NM-Lipo, Leo, Leo@Lipo, Leo@NM-Lipo L (membrane protein-to-lipid weight ratio 1:100), and Leo@NM-Lipo H (membrane protein-to-lipid weight ratio 1:10) were administered through the tail vein respectively (equivalent Leo dose at 10 mg kg^{-1} every day). Rats in the sham group underwent the same anesthesia and artery exposure procedure except the suture insertion.

5.14. In vivo biodistribution

Lipo-DiD, NM-Lipo-DiD (1:100), NM-Lipo-DiD (1:10), and NM-Lipo-DiD (1:1) were injected to the tMCAO rats through the tail vein 0.5 h after the reperfusion at 0.1 mg kg^{-1}. To test the targeting ability of nanosystems to the cerebral ischemic lesion, the brains of tMCAO rats were analyzed through the imaging system 2 h, 6 h, and 12 h postinjection. The sham group was administered with NM-Lipo-DiD (1:10) as a control. The biodistribution of nanosystems in major organs of the heart, liver, spleen, lung, and kidney was evaluated 6 h postinjection by calculating the fluorescence intensity with an *in vivo* imaging system (FX Pro, Bruker, Germany).

5.15. Infarct volume and neurological deficits

The neurological functions of rats were measured using the Longa scoring method at 24 h, 48 h, and 72 h after injection [70], and the neurological deficit scores were blindly graded by two researchers: grade 0, no neurological impairment; grade 1, unable to fully extend the paralyzed forelimb, mild neurological impairment; grade 2, turned to the side of paralysis when walking, moderate nerve function deficit; grade 3, mild dumping to the paralyzed side, severe neurological impairment; grade 4, unable to walk spontaneously, conscious loss. In addition, rat brains were collected and cut into 2 mm-thick sections coronally. Afterward, the brain sections were stained with 1% 2, 3, 5-triphenyltetrazolium chloride (TTC) at 37 °C for 20 min for imaging and quantitative analysis. The percentage of infarct volume was calculated as follows:

$$\text{infarct volume } (\%) = \frac{\textit{infarct area}}{\textit{total coronal section area}} \times 100\% \qquad (6)$$

5.16. Apoptosis analysis

TdT-mediated dUTP nick-end labeling (TUNEL) assays (Beyotime Biotechnology, C1089, China) were performed to detect the neuronal apoptosis in the ischemic regions. The brain slices were treated with 4% PFA, 0.1% Triton X-100 and proteinase k, and washed three times with PBS, followed by counterstaining nuclei with DAPI. Fluorescent images were obtained with a confocal microscope (Leica TCS SP8).

5.17. Evaluation of BBB integrity

BBB disruption was evaluated by Evans blue (EB) test. After administration with PBS, NM-Lipo, Leo, Leo@Lipo, Leo@NM-Lipo L (NM: Lipo = 1:100), and Leo@NM-Lipo H (NM: Lipo = 1:10) (equivalent Leo dose at 10 mg kg^{-1} every day), the tMCAO model rats were injected intravenously with EB dye (40 mg kg^{-1}). After 24 h, the rats were anesthetized and perfused with PBS, and the brains were collected and sectioned for imaging. The ischemic hemispheres were placed in 50% trichloroacetic acid solution to precipitate protein and the supernatant was diluted 4-fold with ethanol. The quantity of EB dye was measured by a microplate reader ($\lambda_{excitation/emission} = 620/680$ nm). To analyze the level of tight junctions-related proteins including Occludin and Claudin 5, the proteins were extracted from and quantified by western blots.

5.18. Inflammatory cytokines detections

The ischemic hemispheres of the brain were weighed, homogenized with PBS containing protease inhibitors (1:10, w/w) on ice and centrifuged at 5000 rpm for 15 min. The supernatant was harvested to quantify the protein level with BCA protein quantification kit and the level of TNF-α, IL-10, and IL-1β were determined with Enzyme-Linked Immunosorbent Assay (ELISA) kits.

5.19. ROS, MDA, and SOD measurements in vivo

To measure the level of ROS in the ischemic hemisphere, single cell suspension of brain tissue at 1×10^6 mL^{-1} was obtained after digestion with trypsin at 37 °C for 30 min and centrifugation at 500g for 10 min, which was incubated with 50 μM DCFHDA at 37 °C for 30 min. Then cells were rinsed with PBS for 3 times and the fluorescence intensity was assayed by a microplate reader ($\lambda_{excitation/emission} = 485/525$ nm). The supernatant of brain homogenization was prepared and the level of MDA and SOD was detected. The brains were rinsed, homogenized with PBS (1:10, w/w) on ice and centrifuged at 5000 rpm for 15 min. The supernatant was harvested at 4 °C to quantify the protein level with BCA protein quantification kit and the level of SOD and MDA levels were measured using assay kits according to the instructions.

5.20. Immunofluorescent and immunohistochemistry staining

Brain sections were sliced at 10 μm by a cryostat (Leica, CM1900), treated with 4% PFA and 0.1% Triton X-100 and washed three times with PBS. For immunohistochemical staining, the sections were blocked with 3% BSA for 30 min, washed 3 times, and incubated with anti-Iba-1 antibody (1:500) and anti-GFAP antibody (1:500) overnight at 4 °C. Then the slices were incubated with corresponding biotin-labeled IgG for 15 min and washed 3 times with PBS. Afterward, the slices were incubated with horseradish peroxidase (HRP) labeled chain enzyme ovalbumin working solution for 15 min and washed 3 times with PBS. After incubation with DAB solution for 5 min, the slices were counterstained with hematoxylin and imaged using an optical microscope.

For immunofluorescent staining, the sections were incubated with proteinase k for 30 min after being blocked with 3% BSA and incubated with anti-8-OHG antibody (1:500) overnight at 4 °C. Alexa Fluor 488-labeled secondary antibody (1:1000) was used for incubation for 30 min at room temperature. After being washed 3 times with PBS, the slices

were counterstained with DAPI, observed by a confocal microscope (Leica TCS SP8), and analyzed by ImageJ.

5.21. Western blot analysis

The ischemic hemisphere of the tMCAO rat was collected 72 h post perfusion, and total protein was extracted with RIPA lysis buffer containing protease inhibitors and quantified using the BCA Protein Assay Kit (Beyotime Biotechnology). The samples were separated by SDS-PAGE and transferred to PVDF membranes. Then the membranes were blocked with 5% nonfat milk powder and incubated with anti-Occludin (1:1000), anti-Claudin 5 (1:1000), anti-Bax (1:1000) anti-Bcl2, anti–HIF–1α (1:1000) and anti-β-actin (1:1000) at 4 °C overnight, followed by HRP-conjugated secondary antibody at room temperature for 1 h. ImageJ was used to analyze the optical density of bands. Quantification of band optical density relative to β-Actin was performed using ImageJ software.

5.22. In vivo safety evaluations

To investigate the preliminary safety of biomimetic nanoliposomes, the body weights of tMCAO rats were monitored at 0, 24, 48, and 72 h after reperfusion. Besides, major organ tissues (heart, liver, spleen, kidney, lung) and blood samples were collected at 72 h post-injection. The paraffin-embedded organ samples were sectioned at a thickness of 5 μm and stained with hematoxylin and eosin (H&E) for visualization under the microscope. Finally, the blood samples were centrifuged and the serum was aspirated for the detection of alanine transaminase (ALT), aspartate aminotransferase (AST), creatinine (CRE), and blood urea nitrogen (BUN) to study the impact of nanoliposomes on liver and kidney function.

6. Statistical analysis

All the data were presented as mean $\pm$ SD. The statistical analysis was processed using Student's t-test or one-way analysis of variance (ANOVA). All the data were analyzed by GraphPad Prism 8 software (GraphPad, San Diego, CA) and the graphs were generated by Origin 9 (OriginLab Corporation, MA, USA). $P < 0.05$ was deemed statistically significant.

Author contributions

Zhuang Tang: Conceptualization, Data Curation, Formal analysis, Investigation, Methodology, Project administration, Validation, Visualization, Writing - original draft, Writing - review & editing; **Shiyu Meng:** Investigation, Methodology, Validation; **Zhiling Song:** Investigation, Methodology; **Xiaoxue Yang:** Investigation, Validation; **Xinzhi Li:** Investigation, Methodology; **Hui Guo:** Funding Acquisition, Resources, Supervision; **Meirong Du:** Funding Acquisition, Resources, Supervision; **Jun Chen:** Conceptualization, Methodology, Supervision; **Yi Zhun Zhu:** Funding Acquisition, Resources, Supervision, Writing - review & editing; **Xiaolin Wang:** Conceptualization, Funding Acquisition, Project administration, Resources, Supervision, Validation, Visualization, Writing - review & editing.

Declaration of competing interest

The authors declare that they have no known competing financial interests or personal relationships that could have appeared to influence the work reported in this paper.

Data availability

Data will be made available on request.

Appendix A. Supplementary data

Supplementary data to this article can be found online at https://doi.org/10.1016/j.mtbio.2023.100674.

References

[1] C.W. Tsao, A.W. Aday, Z.I. Almarzooq, A. Alonso, A.Z. Beaton, M.S. Bittencourt, A.K. Boehme, A.E. Buxton, A.P. Carson, Y. Commodore-Mensah, M.S.V. Elkind, K.R. Evenson, C. Eze-Nliam, J.F. Ferguson, G. Generoso, J.E. Ho, R. Kalani, S.S. Khan, B.M. Kissela, K.L. Knutson, D.A. Levine, T.T. Lewis, J. Liu, M.S. Loop, J. Ma, M.E. Mussolino, S.D. Navaneethan, A.M. Perak, R. Poudel, M. Rezk-Hanna, G.A. Roth, E.B. Schroeder, S.H. Shah, E.L. Thacker, L.B. VanWagner, S.S. Virani, J.H. Voecks, N.Y. Wang, K. Yaffe, S.S. Martin, Heart disease and stroke statistics-2022 update: a report from the American heart association, Circulation 145 (2022) e153–e639.
[2] B.C.V. Campbell, P. Khatri, Stroke, Lancet. 396 (2020) 129–142.
[3] M.S. Phipps, C.A. Cronin, Management of acute ischemic stroke, Br. Med. J. 368 (2020) l6983.
[4] S.J. Mendelson, S. Prabhakaran, Diagnosis and management of transient ischemic attack and acute ischemic stroke: a review, JAMA 325 (2021) 1088–1098.
[5] L. Wang, B. Zhang, X. Yang, S. Guo, G.I.N. Waterhouse, G. Song, S. Guan, A. Liu, L. Cheng, S. Zhou, Targeted alleviation of ischemic stroke reperfusion via atorvastatin-ferritin Gd-layered double hydroxide, Bioact. Mater. 20 (2023) 126–136.
[6] X. Li, Z. Han, T. Wang, C. Ma, H. Li, H. Lei, Y. Yang, Y. Wang, Z. Pei, Z. Liu, L. Cheng, G. Chen, Cerium oxide nanoparticles with antioxidative neurorestoration for ischemic stroke, Biomaterials 291 (2022), 121904.
[7] J.P. Marto, D. Strambo, F. Livio, P. Michel, Drugs associated with ischemic stroke: a review for clinicians, Stroke 52 (2021) e646–e659.
[8] P. Hao, F. Jiang, J. Cheng, L. Ma, Y. Zhang, Y. Zhao, Traditional Chinese medicine for cardiovascular disease: evidence and potential mechanisms, J. Am. Coll. Cardiol. 69 (2017) 2952–2966.
[9] E. Kupeli Akkol, I. Tatli Cankaya, G. Seker Karatoprak, E. Carpar, E. Sobarzo-Sanchez, R. Capasso, Natural compounds as medical strategies in the prevention and treatment of psychiatric disorders seen in neurological diseases, Front. Pharmacol. 12 (2021), 669638.
[10] Y.Z. Zhu, W. Wu, Q. Zhu, X. Liu, Discovery of Leonuri and therapeutical applications: from bench to bedside, Pharmacol. Ther. 188 (2018) 26–35.
[11] K.P. Loh, J. Qi, B.K. Tan, X.H. Liu, B.G. Wei, Y.Z. Zhu, Leonurine protects middle cerebral artery occluded rats through antioxidant effect and regulation of mitochondrial function, Stroke 41 (2010) 2661–2668.
[12] Q.Y. Zhang, Z.J. Wang, D.M. Sun, Y. Wang, P. Xu, W.J. Wu, X.H. Liu, Y.Z. Zhu, Novel therapeutic effects of leonurine on ischemic stroke: new mechanisms of BBB integrity, Oxid. Med. Cell. Longev. 2017 (2017), 7150845.
[13] Q.Y. Zhang, Z.J. Wang, L. Miao, Y. Wang, L. Chang, W. Guo, Y.Z. Zhu, Neuroprotective effect of SCM-198 through stabilizing endothelial cell function, Oxid. Med. Cell. Longev. 2019 (2019), 7850154.
[14] Z.Y. Hong, X.R. Shi, K. Zhu, T.T. Wu, Y.Z. Zhu, SCM-198 inhibits microglial overactivation and attenuates Abeta(1-40)-induced cognitive impairments in rats via JNK and NF-small ka, CyrillicB pathways, J. Neuroinflammation 11 (2014) 147.
[15] S. Zhang, Y. Zhou, R. Li, Z. Chen, X. Fan, Advanced drug delivery system against ischemic stroke, J. Contr. Release 344 (2022) 173–201.
[16] R.H. Fang, A.V. Kroll, W. Gao, L. Zhang, Cell membrane coating nanotechnology, Adv. Mater. 30 (2018), e1706759.
[17] R. Zhang, S. Wu, Q. Ding, Q. Fan, Y. Dai, S. Guo, Y. Ye, C. Li, M. Zhou, Recent advances in cell membrane-camouflaged nanoparticles for inflammation therapy, Drug Deliv. 28 (2021) 1109–1119.
[18] V. Chugh, K. Vijaya Krishna, A. Pandit, Cell membrane-coated mimics: a methodological approach for fabrication, characterization for therapeutic applications, and challenges for clinical translation, ACS Nano 15 (2021) 17080–17123.
[19] G.C. Jickling, D. Liu, B.P. Ander, B. Stamova, X. Zhan, F.R. Sharp, Targeting neutrophils in ischemic stroke: translational insights from experimental studies, J. Cerebr. Blood Flow Metabol. 35 (2015) 888–901.
[20] C. Chen, T. Huang, X. Zhai, Y. Ma, L. Xie, B. Lu, Y. Zhang, Y. Li, Z. Chen, J. Yin, P. Li, Targeting neutrophils as a novel therapeutic strategy after stroke, J. Cerebr. Blood Flow Metabol. 41 (2021) 2150–2161.
[21] S.S. Liu, J.P. Xu, Y.P. Liu, Y. You, L.Z. Xie, S.Q. Tong, Y. Chen, K.F. Liang, S.L. Zhou, F.A. Li, Z. Tang, N. Mei, H.P. Lu, X.L. Wang, X.L. Gao, J. Chen, Neutrophil-biomimetic "nanobuffer" for remodeling the microenvironment in the infarct core and protecting neurons in the penumbra via neutralization of detrimental factors to treat ischemic stroke, ACS Appl. Mater. Interfaces 14 (2022) 27743–27761.

[22] X. Dong, J. Gao, C.Y. Zhang, C. Hayworth, M. Frank, Z. Wang, Neutrophil membrane-derived nanovesicles alleviate inflammation to protect mouse brain injury from ischemic stroke, ACS Nano 13 (2019) 1272–1283.

[23] Y. Yin, W. Tang, X. Ma, L. Tang, Y. Zhang, M. Yang, F. Hu, G. Li, Y. Wang, Biomimetic neutrophil and macrophage dual membrane-coated nanoplatform with orchestrated tumor-microenvironment responsive capability promotes therapeutic efficacy against glioma, Chem. Eng. J. 433 (2022) 133848.

[24] Q. Zhang, D. Dehaini, Y. Zhang, J. Zhou, X. Chen, L. Zhang, R.H. Fang, W. Gao, L. Zhang, Neutrophil membrane-coated nanoparticles inhibit synovial inflammation and alleviate joint damage in inflammatory arthritis, Nat. Nanotechnol. 13 (2018) 1182–1190.

[25] L. Liu, X. Bai, M.V. Martikainen, A. Karlund, M. Roponen, W. Xu, G. Hu, E. Tasciotti, V.P. Lehto, Cell membrane coating integrity affects the internalization mechanism of biomimetic nanoparticles, Nat. Commun. 12 (2021), 127296.

[26] Z. Liu, F. Wang, X. Liu, Y. Sang, L. Zhang, J. Ren, X. Qu, Cell membrane-camouflaged liposomes for tumor cell-selective glycans engineering and imaging in vivo, Proc. Natl. Acad. Sci. U. S A 118 (2021), e2022769118.

[27] S. Shah, V. Dhawan, R. Holm, M.S. Nagarsenker, Y. Perrie, Liposomes: advancements and innovation in the manufacturing process, Adv. Drug Deliv. Rev. 154–155 (2020) 102–122.

[28] D. Pentak, Alternative methods of determining phase transition temperatures of phospholipids that constitute liposomes on the example of DPPC and DMPC, Thermochim. Acta 584 (2014) 36–44.

[29] T. Chen, S.H. Dai, X. Li, P. Luo, Z. Zhu, Y.H. Wang, Z. Fei, X.F. Jiang, Sirt1-Sirt3 axis regulates human blood-brain barrier permeability in response to ischemia, Redox Biol. 14 (2018) 229–236.

[30] D. Chu, X. Dong, X. Shi, C. Zhang, Z. Wang, Neutrophil-based drug delivery systems, Adv. Mater. 30 (2018), e1706245.

[31] Y. Song, N. Zhang, Q. Li, J. Chen, Q. Wang, H. Yang, H. Tan, J. Gao, Z. Dong, Z. Pang, Z. Huang, J. Qian, J. Ge, Biomimetic liposomes hybrid with platelet membranes for targeted therapy of atherosclerosis, Chem. Eng. J. 408 (2021), 127296.

[32] Y. Bi, W. Duan, J. Chen, T. You, S. Li, W. Jiang, M. Li, G. Wang, X. Pan, J. Wu, D. Liu, J. Li, Y. Wang, Neutrophil decoys with anti-inflammatory and anti-oxidative properties reduce secondary spinal cord injury and improve neurological functional recovery, Adv. Funct. Mater. 31 (2021), 2102912.

[33] H. Wang, Y. Liu, R. He, D. Xu, J. Zang, N. Weeranoppanant, H. Dong, Y. Li, Cell membrane biomimetic nanoparticles for inflammation and cancer targeting in drug delivery, Biomater. Sci. 8 (2020) 552–568.

[34] H. Lizhen, H. Guanning, L. Hongxing, S. Chengcheng, L. Xinxin, T. Chen, Highly bioactive zeolitic imidazolate framework-8–capped nanotherapeutics for efficient reversal of reperfusion-induced injury in ischemic stroke, Sci. Adv. 6 (2020), eaay9751.

[35] S.R. Zhang, T.G. Phan, C.G. Sobey, Targeting the immune system for ischemic stroke, Trends Pharmacol. Sci. 42 (2021) 96–105.

[36] R.L. Jayaraj, S. Azimullah, R. Beiram, F.Y. Jalal, G.A. Rosenberg, Neuroinflammation: friend and foe for ischemic stroke, J. Neuroinflammation 16 (2019) 142.

[37] Z.S. Al-Ahmady, D. Jasim, S.S. Ahmad, R. Wong, M. Haley, G. Coutts, I. Schiessl, S.M. Allan, K. Kostarelos, Selective liposomal transport through blood brain barrier disruption in ischemic stroke reveals two distinct therapeutic opportunities, ACS Nano 13 (2019) 12470–12486.

[38] Q.Y. He, Y.Z. Ma, J. Liu, D.H. Zhang, J.X. Ren, R.Y. Zhao, J.L. Chang, Z.N. Guo, Y. Yang, Biological functions and regulatory mechanisms of hypoxia-inducible factor-1 alpha in ischemic stroke, Front. Immunol. 12 (2021), 801985.

[39] Y. Zhang, Y. Liu, Q. Cui, Z. Fu, H. Yu, A. Liu, J. Liu, X. Qin, S. Ge, Q. Zhang, Hydroxysafflor yellow A alleviates ischemic stroke in rats via HIF-1α, BNIP3, and notch1-mediated inhibition of autophagy, Am. J. Chin. Med. 50 (2022) 799–815.

[40] L. Xue, H. Chen, K. Lu, J. Huang, H. Duan, Y. Zhao, Clinical significance of changes in serum neuroglobin and HIF-1alpha concentrations during the early-phase of acute ischemic stroke, J. Neurol. Sci. 375 (2017) 52–57.

[41] C.C. Tsao, J. Baumann, S.F. Huang, D. Kindler, A. Schroeter, N. Kachappilly, M. Gassmann, M. Rudin, O.O. Ogunshola, Pericyte hypoxia-inducible factor-1 (HIF-1) drives blood-brain barrier disruption and impacts acute ischemic stroke outcome, Angiogenesis 24 (2021) 823–842.

[42] V.L. Feigin, M. Brainin, B. Norrving, S. Martins, R.L. Sacco, W. Hacke, M. Fisher, J. Pandian, P. Lindsay, World stroke organization (WSO): global stroke fact sheet 2022, Int. J. Stroke 17 (2022) 18–29.

[43] S. Paul, E. Candelario-Jalil, Emerging neuroprotective strategies for the treatment of ischemic stroke: an overview of clinical and preclinical studies, Exp. Neurol. 335 (2021) 113518.

[44] W. He, Z. Zhang, X. Sha, Nanoparticles-mediated emerging approaches for effective treatment of ischemic stroke, Biomaterials 277 (2021), 121111.

[45] R. Tenchov, R. Bird, A.E. Curtze, Q. Zhou, Lipid nanoparticles-from liposomes to mRNA vaccine delivery, a landscape of research diversity and advancement, ACS Nano 15 (2021) 16982–17015.

[46] D.J.A. Crommelin, P. van Hoogevest, G. Storm, The role of liposomes in clinical nanomedicine development. What now? Now what? J. Contr. Release 318 (2020) 256–263.

[47] W. Lv, J. Xu, X. Wang, X. Li, Q. Xu, H. Xin, Bioengineered boronic ester modified dextran polymer nanoparticles as reactive oxygen species responsive nanocarrier for ischemic stroke treatment, ACS Nano 12 (2018) 5417–5426.

[48] M. Li, J. Li, J. Chen, Y. Liu, X. Cheng, F. Yang, N. Gu, Platelet membrane biomimetic magnetic nanocarriers for targeted delivery and in situ generation of nitric oxide in early ischemic stroke, ACS Nano 14 (2020) 2024–2035.

[49] C. Li, Z. Zhao, Y. Luo, T. Ning, P. Liu, Q. Chen, Y. Chu, Q. Guo, Y. Zhang, W. Zhou, H. Chen, Z. Zhou, Y. Wang, B. Su, H. You, T. Zhang, X. Li, H. Song, C. Li, T. Sun, C. Jiang, Macrophage-disguised manganese dioxide nanoparticles for neuroprotection by reducing oxidative stress and modulating inflammatory microenvironment in acute ischemic stroke, Adv. Sci. 8 (2021), e2101526.

[50] J. Shi, Y. Yang, N. Yin, C. Liu, Y. Zhao, H. Cheng, T. Zhou, Z. Zhang, K. Zhang, Engineering CXCL12 biomimetic decoy-integrated versatile immunosuppressive nanoparticle for ischemic stroke therapy with management of overactivated brain immune microenvironment, Small Methods 6 (2022), e2101158.

[51] W. He, Q. Mei, J. Li, Y. Zhai, Y. Chen, R. Wang, E. Lu, X.Y. Zhang, Z. Zhang, X. Sha, Preferential targeting cerebral ischemic lesions with cancer cell-inspired nanovehicle for ischemic stroke treatment, Nano Lett. 21 (2021) 3033–3043.

[52] J. Chen, Y. Song, Q. Wang, Q. Li, H. Tan, J. Gao, N. Zhang, X. Weng, D. Sun, W. Yakufu, Z. Wang, J. Qian, Z. Pang, Z. Huang, J. Ge, Targeted neutrophil-mimetic liposomes promote cardiac repair by adsorbing proinflammatory cytokines and regulating the immune microenvironment, J. Nanobiotechnol. 20 (2022) 218.

[53] L. Feng, C. Dou, Y. Xia, B. Li, M. Zhao, P. Yu, Y. Zheng, A.M. El-Toni, N.F. Atta, A. Galal, Y. Cheng, X. Cai, Y. Wang, F. Zhang, Neutrophil-like cell-membrane-coated nanozyme therapy for ischemic brain damage and long-term neurological functional recovery, ACS Nano 15 (2021) 2263–2280.

[54] C. Zhang, L. Zhang, W. Wu, F. Gao, R.Q. Li, W. Song, Z.N. Zhuang, C.J. Liu, X.Z. Zhang, Artificial super neutrophils for inflammation targeting and HclO generation against tumors and infections, Adv. Mater. 31 (2019), e1901179.

[55] H.-N. Yu, Y.-R. Lee, E.-M. Noh, K.-S. Lee, E.-K. Song, M.-K. Han, Y.-C. Lee, C.-Y. Yim, J. Park, B.-S. Kim, I.-H. Lee, S.J. Lee, J.-S. Kim, Tumor necrosis factor-α enhances DMSO-induced differentiation of HL-60 cells through the activation of ERK/MAPK pathway, Int. J. Hematol. 87 (2008) 189–194.

[56] D. Wang, S. Wang, Z. Zhou, D. Bai, Q. Zhang, X. Ai, W. Gao, L. Zhang, White blood cell membrane-coated nanoparticles: recent development and medical applications, Adv. Healthcare Mater. 11 (2022), e2101349.

[57] X. Xue, H. Liu, S. Wang, Y. Hu, B. Huang, M. Li, J. Gao, X. Wang, J. Su, Neutrophil-erythrocyte hybrid membrane-coated hollow copper sulfide nanoparticles for targeted and photothermal/anti-inflammatory therapy of osteoarthritis, Compos. B Eng. 237 (2022), 109855.

[58] R. Molinaro, C. Corbo, J.O. Martinez, F. Taraballi, M. Evangelopoulos, S. Minardi, I.K. Yazdi, P. Zhao, E. De Rosa, M.B. Sherman, A. De Vita, N.E. Toledano Furman, X. Wang, A. Parodi, E. Tasciotti, Biomimetic proteolipid vesicles for targeting inflamed tissues, Nat. Mater. 15 (2016) 1037–1046.

[59] H. Liu, X. Zhang, Y. Du, H. Ji, S. Li, L. Li, Y. Xing, X. Zhang, L. Dong, C. Wang, K. Zhao, Y. Ji, X. Cao, Leonurine protects brain injury by increased activities of UCP4, SOD, CAT and Bcl-2, decreased levels of MDA and Bax, and ameliorated ultrastructure of mitochondria in experimental stroke, Brain Res. 1474 (2012) 73–81.

[60] N. Letko Khait, E. Ho, M.S. Shoichet, Wielding the double-edged sword of inflammation: building biomaterial-based strategies for immunomodulation in ischemic stroke treatment, Adv. Funct. Mater. 31 (2021), 2010674.

[61] X. Jiang, A.V. Andjelkovic, L. Zhu, T. Yang, M.V.L. Bennett, J. Chen, R.F. Keep, Y. Shi, Blood-brain barrier dysfunction and recovery after ischemic stroke, Prog. Neurobiol. 163–164 (2018) 144–171.

[62] Q. He, Y. Ma, J. Liu, D. Zhang, J. Ren, R. Zhao, J. Chang, Z.N. Guo, Y. Yang, Biological functions and regulatory mechanisms of hypoxia-inducible factor-1alpha in ischemic stroke, Front. Immunol. 12 (2021), 801985.

[63] F. Yang, D. Zhao, D. Wang, Z. Wang, Q.Y. Huang, Minocycline ameliorates hypoxia-induced blood-brain barrier damage by inhibition of HIF-1alpha through SIRT-3/PHD-2 degradation pathway, Neuroscience 304 (2015) 250–259.

[64] T. Kang, Q. Zhu, D. Wei, J. Feng, J. Yao, T. Jiang, Q. Song, X. Wei, H. Chen, X. Gao, J. Chen, Nanoparticles coated with neutrophil membranes can effectively treat cancer metastasis, ACS Nano 11 (2017) 1397–1411.

[65] J. Xue, Z. Zhao, L. Zhang, L. Xue, S. Shen, Y. Wen, Z. Wei, L. Wang, L. Kong, H. Sun, Q. Ping, R. Mo, C. Zhang, Neutrophil-mediated anticancer drug delivery for suppression of postoperative malignant glioma recurrence, Nat. Nanotechnol. 12 (2017) 692–700.

[66] X. Zhou, X. Cao, H. Tu, Z.R. Zhang, L. Deng, Inflammation-targeted delivery of celastrol via neutrophil membrane-coated nanoparticles in the management of acute pancreatitis, Mol. Pharm. 16 (2019) 1397–1405.

[67] H. Cao, Z. Dan, X. He, Z. Zhang, H. Yu, Q. Yin, Y. Li, Liposomes coated with isolated macrophage membrane can target lung metastasis of breast cancer, ACS Nano 10 (2016) 7738–7748.

[68] Q. Yuan, J.X. Wang, R.L. Li, Z.Z. Jia, S.X. Wang, H. Guo, L.J. Chai, L.M. Hu, Effects of salvianolate lyophilized injection combined with Xueshuantong injection in regulation of BBB function in a co-culture model of endothelial cells and pericytes, Brain Res. 1751 (2021), 147185.

[69] C.J. Sommer, Ischemic stroke: experimental models and reality, Acta Neuropathol. 133 (2017) 245–261.

[70] J.R. Zhu, H.D. Lu, C. Guo, W.R. Fang, H.D. Zhao, J.S. Zhou, F. Wang, Y.L. Zhao, Y.M. Li, Y.D. Zhang, C.Q. Yang, J.G. Sun, Berberine attenuates ischemia-reperfusion injury through inhibiting HMGB1 release and NF-kappaB nuclear translocation, Acta Pharmacol. Sin. 39 (2018) 1706–1715.